HYBRID MODEL FOR PROBE-FED RECTANGULAR MICROSTRIP ANTENNAS WITH SHORTING STRIPS

A THESIS
SUBMITTED TO THE DEPARTMENT OF ELECTRICAL AND
ELECTRONICS ENGINEERING
AND THE INSTITUTE OF ENGINEERING AND SCIENCES
OF BILKENT UNIVERSITY
IN PARTIAL FULFILLMENT OF THE REQUIREMENTS
FOR THE DEGREE OF
MASTER OF SCIENCE

BY

SELMA MUTLU

JANUARY 2001

HYBRID MODEL FOR PROBE-FED RECTANGULAR MICROSTRIP ANTENNAS WITH SHORTING STRIPS

A THESIS

SUBMITTED TO THE DEPARTMENT OF ELECTRICAL AND

ELECTRONICS ENGINEERING

AND THE INSTITUTE OF ENGINEERING AND SCIENCES

OF BILKENT UNIVERSITY

IN PARTIAL FULFILLMENT OF THE REQUIREMENTS

FOR THE DEGREE OF

MASTER OF SCIENCE

By

Selma Mutlu

January 2001

I certify that I have read this thesis and that in my opinion it is fully adequate, in scope and in quality, as a thesis for the degree of Master of Science.

Prof. Dr. M. İrşadi Aksun (Supervisor)

I certify that I have read this thesis and that in my opinion it is fully adequate, in scope and in quality, as a thesis for the degree of Master of Science.

Prof. Dr. Ayhan Altıntaş

I certify that I have read this thesis and that in my opinion it is fully adequate, in scope and in quality, as a thesis for the degree of Master of Science.

Asst. Prof. Dr. Lale Alatan

Approved for the Institute of Engineering and Sciences:

Prof. Dr. Mehmet Baray
Director of Institude of Engineering and Sciences

ABSTRACT

HYBRID MODEL FOR PROBE-FED RECTANGULAR MICROSTRIP ANTENNAS WITH SHORTING STRIPS

Selma Mutlu

M.S. in Electrical and Electronics Engineering

Supervisor: Prof. Dr. M. İrşadi Aksun

January 2001

In the dual frequency operation of microstrip antennas, shorting strips are used to adjust the ratio of frequencies. A multi-port analysis is usually employed to predict the input impedance and resonant frequency of probe-fed microstrip antennas with shorting strips. However, this approach does not provide any information about the field distribution under the patch. In this thesis, a hybrid model, using both the cavity model and point matching, is developed to calculate the field distribution under the patch with shorting pins and strips. In addition, this model also accounts for the conducting nature of the feed and shorting strips, with the help of the point-matching algorithm. Then, to verify the model, the theoretical results obtained from the hybrid method are compared to the experimental results and good agreement is observed. Finally, a genetic algorithm is developed for optimizing the position and width of the shorting strips to achieve desired frequency ratio and input impedances in dual-band operations.

Keywords: Cavity model, dual frequency operation, shorting strips, multi-port analysis, genetic algorithm.

ÖZET

MİL BESLEMELİ KISA-DEVRELEYİCİ ŞERİTLİ DİKDÖRTGENSEL KÜÇÜK-ŞERİT ANTENLER İÇİN GELİŞTİRİLMİŞ BİLEŞKE MODEL

Selma Mutlu
Elektrik ve Elektronik Mühendisliği Bölümü Yüksek Lisans
Tez Yöneticisi: Prof. Dr. M. İrşadi Aksun
Ocak 2001

Kısa-devreleyici şeritler, küçük-şerit antenlerin çift bandlı çalışmasında frekans oranlarını ayarlamak için kullanılırlar. Mil beslemeli, kısa-devreleyici şeritli küçük-şerit antenlerin giriş dirençlerini ve rezonans frekanslarını bulmada yaygın olarak kullanılan metod çoklu giriş-çıkış teorisidir. Ancak, bu yaklaşım, yama altındaki alan dağılımı hakkında bilgi sağlamamaktadır. Bu tezde, kısa-devreleyici iğneli ve şeritli yama altındaki alan dağılımını bulmak için, hem boşluk modelini hem de noktasal denkleştirmeyi kullanan bileşke model geliştirilmiştir. Bu model ayrıca beslemenin ve kısa-devreleyici şeritlerin iletken yapısını da dikkate almaktadır. Daha sonra, bileşke modelin kuramsal sonuçları deneysel sonuçlarla karşılaştırılmış ve sonuçların uygunluğu görülmüştür. Son olarak, istenilen frekans oranı ve giriş direnci değerlerinde çift bandlı işleyişi sağlayacak kısa devreleyici şeritlerin yer ve genişliklerini bulan genetik algoritma geliştirilmiştir.

Anahtar Kelimeler: Boşluk modeli, çift bandlı işleyiş, kısa devreleyici şeritler, çoklu giriş-çıkış teorisi, genetik algoritma.

ACKNOWLEDGMENTS

I would like to express my sincere gratitude to my supervisor Prof. Dr. M. İrşadi Aksun for his supervision, guidance, suggestions, and encouragement throughout the development of this thesis.

I would like to thank the members of my committee, Prof. Dr. Ayhan Altıntaş, Asst. Prof. Dr. Lale Alatan and Dr. Vakur Ertürk for their valuable comments on the thesis.

I would like to extend my thanks to Ergün Hırlakoğlu for his help during the experimental stage of this thesis.

I would like to thank my close friend Özlem Özgün for her support, friendship and love.

Special thanks go to Mehmet Şahin for his love and sincere heart.

Finally, I would like to thank my parents for their endless love, trust, support and encouragement throughout my life.

Contents

List of Figures

List of Tables

Chapter 1

Introduction

The concept of using microstrip antennas as printed radiating structures is a relatively new advance in antenna engineering. Although the fact that printed microstrip structures radiate was brought into light in the mid-50s by Deschamps [1], the application of this idea to design useful antennas started only in 1970s when conformal antennas were desired for missiles. Until then, work done on microstrip antennas was not reported in the literature. In 1970, Byron [2] introduced a conducting strip radiator that was located on a dielectric substrate above a ground plane and fed by coaxial lines along both radiating edges. Following these developments, Munson [3] patented a microstrip element and Howell [4] reported the first data on basic rectangular and circular microstrip patches, hence a new antenna industry was born.

The first mathematical modelling of the basic microstrip radiator was established by Munson [5] and Derneryd [6], in which they applied transmission line concept to rectangular patches fed at the center of radiating edge. Lo *et al.* [7]

introduced the first mathematical analysis of a wide variety of microstrip patches with some canonical shapes, and this approach is now known as the Cavity Model in the literature. In this approach, they used modal expansion technique in the analysis of several patch shapes such as rectangular, circular, semicircular and triangular patches. This was followed by several reports on advanced analysis techniques by Derneryd [8], Shen and Long [9], and Carver and Coffey [10].

By 1978, microstrip patch antennas were widely known and used in communication systems. Along with these developments, a flurry of interest has been concentrated on developing new models and improving existing models to understand the radiation mechanism and to predict the electrical characteristics of such antennas. As a result, the first book on microstrip antennas was published by Artech House in 1980 [11], and since then, there has been lots of scientific articles and books related to microstrip antennas. Even though the properties and theory of these antennas are now rather well-understood [12, 13], there are still significant amount of research on the development of printed antennas for wireless communication systems.

Because of the current revolution in the design of miniaturized electronic circuits, conventional antennas have turned to be bulky and costly part of an electronic system. As alternatives to the conventional antennas, microstrip antennas have attracted great attention in the last few years and find application in several fields [14] due to their unique features:

- Low profile and conformal structure,
- Suitable for mass production (low cost),
- Clarity of radiation characteristics,

- Easy for miniaturization and hence lightweight,
- Structurally robust,
- Direct integrability with microwave circuitry.

Microstrip antennas, recently, have found applications mainly in mobile satellite communication systems such as International Maritime Satellite System (INMARSAT), Mobile Satellite System (MSAT) and IRIDIUM, in Global Positioning Systems (GPS) that enable tracking of individuals, and in Direct Broadcast Satellite Systems (DBS) that are used to provide television services. In addition to these satellite-based applications, microstrip antennas are used in many other areas, which are, namely, the remote-sensing applications, aircraft applications, automobile and microwave sensing applications. For the remote-sensing applications, Synthetic Aperture Radar (SAR) technique is the most important one that determines ground soil grades, vegetation type, ocean wave speed and direction, and predicts the weather. For the aircraft applications, the altimetry, collision avoidance, and remote sensing are some of the examples, while, for the automobiles, the collision avoidance system and microwave sensing alarm systems are the typical examples. In addition to these areas, microstrip antennas are also used in medical area in treating malignant tumours.

Despite their advantages, microstrip antennas suffer from narrow bandwidth (generally less than 3%) and poor radiation efficiency (*power radiated/power input*). To overcome these shortcomings, different modifications onto the microstrip antennas have been developed, some of which, used in combination or alone, are given as follows: use of thicker substrates with low relative dielectric constants; multiple patches either in one plane [15] or stacked vertically [16]; electromagnetically coupled feed geometries; some slot geometries printed on the

patch; and use of broadband impedance matching networks [17]. However, these modifications are not free from problems, for example, increasing the substrate thickness brings about spurious radiation associated with the feed junction and surface wave effects.

To extend the range of applications of microstrip antennas for the systems that require dual-band operations, they are designed to operate for two discrete frequency bands instead of a single wide band. Such antennas are used in GPS, portable mobile communication systems, regional mobile satellite arrays, large feed arrays for offset reflectors, and GSM900 and GSM1800 wireless communications systems that could operate in both bands simultaneously.

Many researchers have studied the dual-frequency operation of microstrip antennas. The first approach was to use two or more patch antennas stacked on top of each other, or placed side by side and interconnect them with transmission lines [18]. This design was essentially a circuit problem, where the design of a circuit minimizing the impedance and radiation pattern interactions between patches was required. The idea of using a single patch in dual-frequency operation was first proposed and realized by Derneryd [19]. He used a single disc-shaped patch that is connected to a complex impedance matching network, which takes as much space and weight as the patch itself. Since a single resonance was split into two narrowly spaced operating bands, both resonances had a narrow band of operation in this design. Since then, a variety of single-patch, dual-band microstrip antennas have been proposed and designed, some of which use patches loaded with shorting pins [20-23] or varactor diodes [24], patches with slots [25-37], patches with slits[38, 39], patches with more than one ports [40, 41], and patch arrays [42].

To understand the mechanism of the dual-band operation of a single microstrip antenna, it is enough to know that these microstrip patches are resonant structures, and they can resonate at many frequencies. The resonant behaviour of the microstrip patches and their radiation mechanisms can be best understood by the Cavity Model, which will be detailed in the following chapters. The dual-frequency operation with just a single patch antenna is only useful if both of the frequency bands of interest have the same radiation pattern, same polarization and same input impedance characteristics, and if there is a single feed for all bands. The two lowest useful modes of resonance satisfying these constraints are (0,1) and (0,3) modes, according to the Cavity Model. In the dual-frequency operation, it is also desired that the two operating frequencies associated with the modes are tunable, that is, the ratio of the two operating frequencies is not fixed. However, (0,1) and (0,3) modes have a fixed ratio of about three. One method to adjust the frequency ratio is to place shorting strips at the nodal lines of (0,3) modal electrical field [21, 22, 43]. These strips increase the operating frequency of (0,1) mode, but have no strong effect on (0,3) modal frequency, since they do not affect the field distribution of (0,3) mode. This makes the (0,1) modal frequency tunable independent of the high band. As a result, one needs to know the effect of the shorting strips on the electrical characteristics of the patches.

To predict the effect of shorting pins, a method called *multi-port analysis* was developed, which mainly depends on the Cavity Model and the concepts of Basic Circuit Theory. It models the shorting pins as additional ports which are terminated in short circuits by setting the voltages at these ports to zero, then finds the Z parameters of the whole system. Hence, one can easily determine the input impedance, and in turn the resonant frequency, of the patch with shorting pins.

Although this approach can predict the important electrical parameters of the antenna, such as the input impedance and resonant frequency, it does not provide any information about the field distribution inside the antenna, which is an important parameter for the calculation of radiation parameters like the radiation pattern and gain. In other words, this method is not able to predict the far zone fields and hence radiation pattern of the microstrip antenna and the related parameters.

In this thesis, a hybrid model is proposed and presented to predict the field distribution under the rectangular patch with shorting pins. This model considers the shorting pins (or strips) as additional current sources with unknown amplitudes. The field under the patch is obtained as a linear superposition of contributions from each source via the Cavity Model. The unknown current densities over the shorting strips are determined using the point matching that implements the boundary condition on the tangential electric field along the shorting strips, which are made of perfect electrical conductors (PEC). This method also forces the electric field under the patch to satisfy the boundary condition on the feeding conductor, which is also made of PEC. It is observed that the results obtained by the hybrid method, proposed in this thesis, agree extremely well with those obtained experimentally. Since it is a natural extension of all analysis tools to be used in the design process, an optimization program, based on the genetic algorithm, is developed. This is to optimize the locations and widths of the shorting strips to get a desired frequency ratio of a dual-band operation, of course with desired input impedances over each band.

The thesis starts with an introduction in Chapter 1, and is followed by the general properties of microstrip antennas, and detailed information about the

cavity model for probe-fed rectangular microstrip antennas in Chapter 2. In Chapter 3, multi-port analysis of microstrip antennas with shorting pins is provided. In Chapter 4, the proposed hybrid model is presented, and then, the theoretical results in comparison with the experimental results are given and discussed in Chapter 5. In Chapter 6, the genetic algorithm for optimization is presented with some results, and the thesis is concluded in Chapter 7.

Chapter 2

Microstrip Antennas and Cavity Model

Since the main topic in this thesis is the development of a novel approach to accurately analyze microstrip antennas with shorting pins and strips, that is, a hybrid method based on the Cavity Model and the point matching approach, this chapter presents some basic information on microstrip antennas and a detailed presentation of the Cavity Model for rectangular probe-fed microstrip antennas. Following the introduction of the Cavity Model, the internal field distribution in the cavity, expressions for the far fields, quality factor, input impedance and resonant frequencies are derived.

2.1 General Information on Microstrip Antennas

A microstrip antenna, also known as patch antenna, is a low-profile printed

antenna, whose basic geometry is illustrated in Figure 2.1. It basically consists of two parallel conducting layers separated by a single thin dielectric substrate, which has a thickness commonly very small in wavelength. The upper conductor is the resonant patch and the lower conductor is the ground plane. Although the shape of the patch is arbitrary, rectangular, circular, equitriangular and annular patches are the most common ones employed in practice. In this thesis, the rectangular patch antennas are analyzed and designed, however the approach presented here is perfectly applicable to other shapes of microstrip antennas.

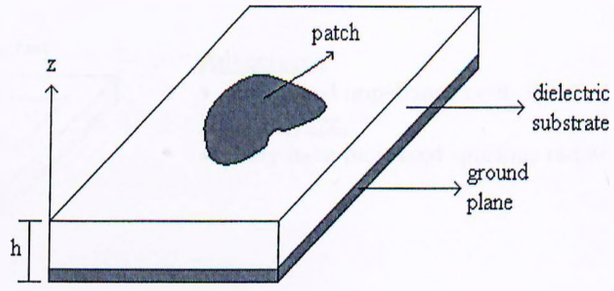

Figure 2.1: Basic geometry of a microstrip patch antenna.

In the design of a microstrip antenna, the most important issue is the design of the feed geometry, which could use a coaxial probe, a microstrip line, or some type of an electromagnetic coupling. Therefore, various feeding structures that are commonly used in the literature, together with their advantages and disadvantages are given in Figure 2.2. Although there are plenty of other feeding geometries, these feeding geometries specially tuned for specific applications are not included here. The emphasis of this thesis is on the coaxial-fed microstrip antenna.

1) Coaxial Feed (Probe Feed)

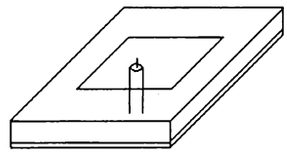

Advantages:
- simple construction
- Little coupling between patch & line
- allows easy impedance control

Disadvantages:
- costly in fabrication, not monolithic
- difficult to incorporate feed boundary condition into analysis
- nonresonant for $h/\lambda_0 >\approx 0.1$

2) Microstrip Feed

a) Edge Feed

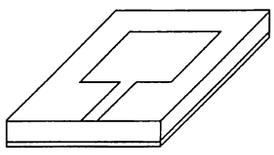

Advantage:
- both patch and feed line can be printed in one step

Disadvantages:
- inflexible in design, since both patch and feed are over the same substrate
- limited impedance control
- spurious radiation from feed line

b) Inset Feed

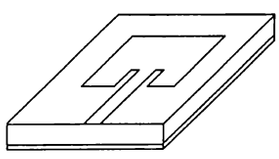

Advantage:
- improved impedance control

Disadvantage:
- may have increased spurious radiation

3) EM Coupling

a) Proximity Coupling

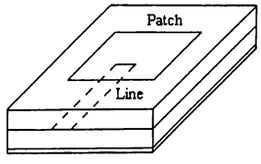

Advantages:
- reduced line radiation
- monolithic

Disadvantage:
- increased complexity

b) Aperture Coupling

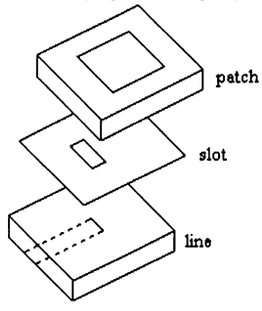

Advantages:
- no interference from feed radiation
- monolithic

Disadvantage:
- increased complexity

Figure 2.2: Feeding methods

In all feeding geometries, a portion of the electromagnetic energy that is guided into the region between the patch and ground plane is radiated from the patch boundary into the space. Since microstrip elements are typically narrow-band antennas, the mismatch between the antenna and the feeding circuitry plays an important role in the efficient excitation of the antenna. In addition, in most applications the bandwidth limitations are due to an impedance mismatch to the feeding circuitry outside of a narrow band. Therefore, one needs to judiciously decide on the type of feeding structure and the location of the feed. It should be remembered that the optimum feed location is not unique, and for some modes of some elements, the suitable feed point can be found on the edge of the patch, while for some others it is impossible to find a location at the edge of the patch. In other words, for some problems it becomes inevitable to use an interior point of the patch for the location of the feed, which can be done by using a coaxial feed geometry.

Once it is decided on the shape of the patch and the form of the feeding structure, one needs to use a suitable method to analyze the antenna in order to be able to design the antenna that satisfies the specifications. There are several methods to analyze microstrip antennas, and they are given as follows:

- Transmission Line Model [5],
- Cavity Model [44-46],
- Method of Moments [47],
- Unimoment Monte Carlo Method [48],
- Finite-Element Technique [49],
- Direct Form of Network Analysis [50],
- Wire-Grid Method [51],

- Segmentation and Desegmentation Technique [52],
- Bergeron's Method [53],
- Finite Difference Time Domain Method [54].

These methods have different levels of complexity, and the guidelines to determine which one of these methods is best to use for the problem at hand are: antenna thickness, antenna geometry, the excitation system and the particular antenna performance to be evaluated.

In this thesis, the proposed approach for the analysis of microstrip antennas is based on the cavity model together with a simple variant of the method of moments, the point matching. Therefore, it would be instructive to review the Cavity Model in detail first.

2.2 Cavity Model (CM)

The Cavity Model was first proposed by Lo, Solomon and Richards in 1979 [46], and further improved by Richards, Lo and Harrison in 1981 [44]. It was originally developed for probe-fed, very thin (compared to wavelength) microstrip antennas, assuming that the fields under the patch are independent of the coordinate axis perpendicular to the ground and the patch conductors (z-direction in Fig. 2.3).

An enclosure completely surrounded by conducting walls is called a cavity, which has discrete, infinitely many natural resonant frequencies. The CM treats a microstrip antenna as a thin cavity enclosed by very high impedance walls on the sides and PECs on the top and bottom. The high impedance condition at the periphery walls implies that E-field tangential to the patch edge is maximum, whereas the H-field tangential to the edge is approximately zero. Thus, the patch

edge can be considered as a perfect magnetic conductor (PMC), and the microstrip and ground planes can be considered as perfect electric conductors (PEC). In other words, CM treats the patch antenna (the region between the microstrip and the ground plane) as a thin cavity, which is bounded by magnetic walls along the edge and by electric walls from above and below as shown in Figure 2.3. Obviously, such a closed cavity would radiate no power, but with the introduction of some tangent loss to the dielectric material inside the cavity that would incorporate not only the loss of the dielectric material but also the radiation loss, the radiation mechanism would have been taken into account. The approximation behind CM is that the field structure in the microstrip antenna is essentially the same as that of the cavity. Once the field distribution is known, the radiation pattern and the total radiated power can be calculated from the electrical field distribution at the periphery of the cavity (behaves like a magnetic current source), and the input impedance at any feed point can be computed from the field distribution in the cavity.

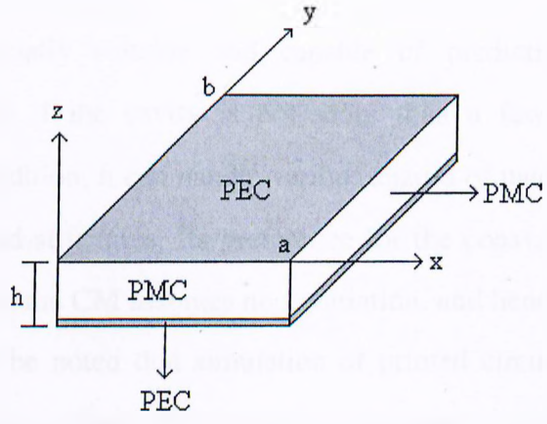

Figure 2.3: Cavity modeling of rectangular patches

As a summary of these discussions, the following assumptions and

approximations, which are inherent in the model, are used in the implementation of the cavity model:

- Due to the close distance between the patch and the ground plane, electric field vector **E** has only z component and magnetic field vector **H** has only x-y components (transverse components) in the region bounded by the microstrip patch and the ground plane. This is the reason why the cavity formed as described above is named as transverse magnetic (TM) cavity.

- Field components in the cavity region are independent of z variable, i.e., they are constants along z-axis.

- Since the electric current on the microstrip patch should have no component normal to the edge at any point along the edge, the tangential **H** field along the edge is zero.

- The existence of fringing fields is taken into account by slightly extending the edges with some heuristic formula.

The CM is especially suitable and capable of predicting the antenna performance accurately if the cavity is not more than a few hundreds of a wavelength thick. In addition, it can handle various shapes of patches, but is most suitable for coaxial feed structures. Its preference for the coaxial feed geometry comes from the fact that the CM assumes no z-variation, and hence no z-variation for the feed. It should be noted that simulation of printed circuits with vertical metalization, such as coaxial feed, shorting strips, via holes, etc., is quite difficult and time consuming with a full-wave approach for layered problems. However, these vertical metalizations are rather easy to incorporate into the formulation of

the CM for a patch problem. Besides, the major advantage of the CM is the fact that it provides physical insight and intuition for the operation of the antenna and for the feeding mechanism and coupling to the modes of the cavity.

There are two different, but equivalent, methods to solve for the field distribution inside the cavity: (i) the resonant mode expansion model; and (ii) expansion using modal matching technique. The resonant mode expansion method expresses the field as a double infinite series of orthogonal mode functions. Each of these mode functions satisfies the source-free wave equation and appropriate boundary conditions, while their linear combination, namely the total field, satisfies the source condition. Modal matching technique solves the homogeneous wave equation in each source-free region. Each source-free solution satisfies all boundary conditions, except at the interface between the two regions where source is located. A complete solution is then determined by matching the solutions to the source. This results in a single infinite series expansion for the field.

The following sections give the details of the determination of the internal field structure, far-zone fields, quality factor and input impedance for a rectangular microstrip patch antenna using the resonant mode expansion. In all these derivations, the geometry shown in Figure 2.4 is used.

2.2.1 Derivation of the Internal Field Distribution via the Resonant Mode Expansion Method

A rectangular microstrip patch antenna (a x b) fed by a coaxial line, having an inner conductor of width d at point (x_p, y_p), with a z-directed current density vector $\mathbf{J}$ is shown in Figure 2.4. It is located over a substrate with a thickness of h and a

dielectric constant of ε_r, and backed by a PEC ground plane.

Starting with Maxwell's equations, with the assumption of sinusoidal time dependence of *exp(jwt)*, we have

$$\nabla \times \mathbf{H} = j\omega\varepsilon\mathbf{E} + \mathbf{J} \tag{2.1}$$

$$\nabla \times \mathbf{E} = -j\omega\mu\mathbf{H} \tag{2.2}$$

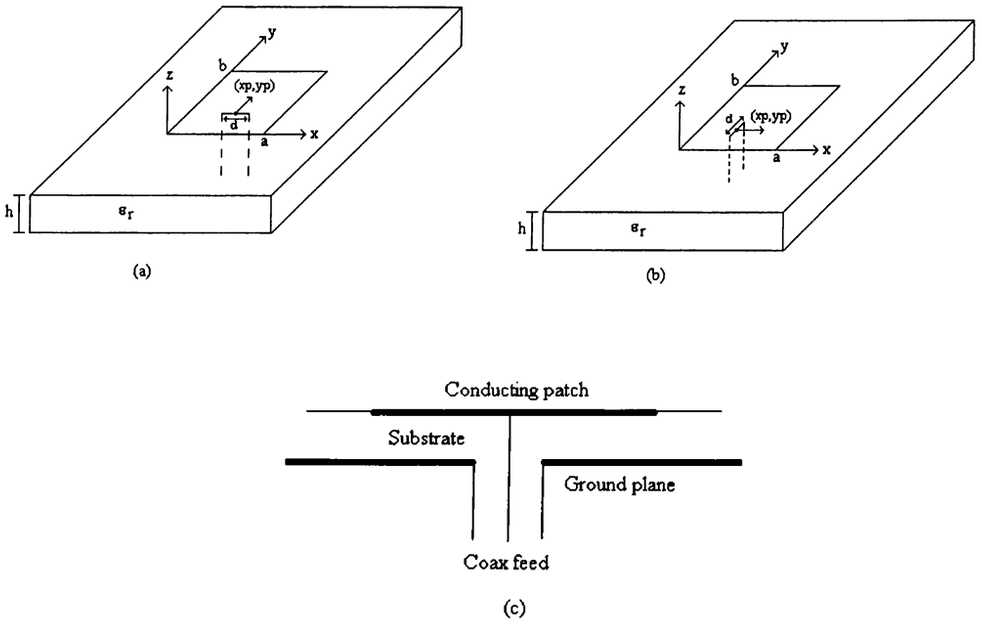

Figure 2.4: Probe-fed rectangular microstrip patch antenna; (a) general view with x-directed probe, (b) general view with y-directed probe, (c) side view.

These two equations can be solved in terms of **E**, which yields the following wave equation:

$$\nabla(\nabla.\mathbf{E}) - \nabla^2\mathbf{E} = \omega^2\mu\varepsilon\mathbf{E} - j\omega\mu\mathbf{J}\,. \tag{2.3}$$

The assumptions of **E** being in the z direction and independent of z imply

$$\nabla.\mathbf{E} = 0 \tag{2.4}$$

then, the wave equation is written as

$$\nabla^2 \mathbf{E} + k^2 \mathbf{E} = j\omega\mu \mathbf{J} \tag{2.5}$$

where

$$k^2 = \omega^2 \mu\varepsilon = k_0{}^2 \varepsilon_r (1 - j\delta), \tag{2.6}$$

$$k_0^2 = \omega^2 \mu\varepsilon_0, \tag{2.7}$$

μ = permeability of free space,

ε_0 = permittivity of free space,

ε_r = relative permittivity of the substrate with respect to ε_0,

δ = loss tangent of the dielectric substrate,

$\mathbf{J}$ = feed current density.

The field inside the cavity can be expressed as a double infinite summation of orthogonal mode functions:

$$\mathbf{E}(x, y) = \hat{\mathbf{z}} E_z = \hat{\mathbf{z}} \sum_m \sum_n C_{mn} \psi_{mn}(x, y). \tag{2.8}$$

where C_{mn}' s are the constant coefficients to be determined. This further simplifies (2.5) into

$$\nabla_t{}^2 E_z + k^2 E_z = j\omega\mu J \tag{2.9}$$

where ∇_t is the transverse to z part of the "del" operator.

Each of the discrete mode functions, which are the eigenfunctions of the cavity, satisfies the homogeneous wave equation

$$\nabla_t{}^2 \psi_{mn} + k_{mn}{}^2 \psi_{mn} = 0 \tag{2.10}$$

and the Neumann boundary condition at the magnetic walls of the cavity,

$$\frac{\partial \psi_{mn}}{\partial \tau} = 0 \tag{2.11}$$

which is also called PMC boundary condition. Here k_{mn} is the cut-off wave number of *(m,n)*th mode and τ is the direction pointing outwards at the PMC

walls.

For the coordinate system of Fig. 2.4, Eq.(2.10) can be written in the following form:

$$\left(\frac{\partial^2}{\partial x^2}+\frac{\partial^2}{\partial y^2}+k_{mn}^2\right)\psi_{mn}=0 \tag{2.12}$$

Using the method of separation of variables, and assuming the solution for k_{mn} as

$$k_{mn}{}^2 = k_x{}^2 + k_y{}^2 , \tag{2.13}$$

ψ_{mn} is obtained as:

$$\psi_{mn}(x,y)=\left(A\sin k_x x+B\cos k_x x\right)\left(C\sin k_y y+D\cos k_y y\right). \tag{2.14}$$

With the application of the PMC boundary conditions at the side-walls of the cavity, the unknown coefficients and the eigenvalues of the mode function, *C, D,* k_x and k_y can be determined:

At $y = 0$: $\dfrac{\partial\psi_{mn}}{\partial y}=0$ implies that $C = 0$.

At $x = 0$: $\dfrac{\partial\psi_{mn}}{\partial x}=0$ implies that $A = 0$.

At $y = b$: $\dfrac{\partial\psi_{mn}}{\partial y}=0$ implies that $k_y=\dfrac{n\pi}{b}$ where $n = 0,1,....$

At $x = a$: $\dfrac{\partial\psi_{mn}}{\partial x}=0$ implies that $k_x=\dfrac{m\pi}{a}$ where $m = 0,1,.....$

Hence, the resulting ψ_{mn} and k_{mn} are obtained as

$$\psi_{mn}(x,y)=\alpha_{mn}\cos\left(\frac{m\pi x}{a}\right)\cos\left(\frac{n\pi y}{b}\right) \tag{2.15}$$

$$k_{mn}=\sqrt{\left(\frac{m\pi}{a}\right)^2+\left(\frac{n\pi}{b}\right)^2} \tag{2.16}$$

where α_{mn} is a constant that is chosen to make ψ_{mn}'s orthonormal

$$\alpha_{mn} = \sqrt{\frac{\varepsilon_{om}\varepsilon_{on}}{ab}} \tag{2.17}$$

and $\varepsilon_{om,on} = \begin{cases} 1 & m,n = 0 \\ 2 & m,n \neq 0 \end{cases}$.

Once the natural modes of the system are found, that is, the homogenous solution of the differential equation (2.12), the forced solution should be obtained with the use of these homogenous solutions. To do so, one needs to remember that Maxwell's equations are linear, and together with the boundary conditions they define a linear system. In addition, Green's functions are the fields due to a point source and used as the impulse response of the system, from which the field distribution due to the actual source can be obtained via the convolution integral. Let G_z be the Green's function representing z-directed electric field inside the cavity due to z-directed impulse source $\tilde{\delta}$ located at (x_p, y_p). It satisfies:

$$\nabla_t^2 G_z + k^2 G_z = \tilde{\delta}(x - x_p)\tilde{\delta}(y - y_p). \tag{2.18}$$

Using the natural modes of the cavity, the solution of the differential equation, G_z, can be written as a linear combination of these orthonormal modes as

$$G_z(x,y) = \sum_m \sum_n A_{mn}\psi_{mn}(x,y) \tag{2.19}$$

where A_{mn}'s are constant coefficients to be determined. The impulse function at the right hand side of Eq.(2.18) can also be written as a superposition of these modes, because the modal functions constitute a complete set:

$$\tilde{\delta}(x - x_p)\tilde{\delta}(y - y_p) = \sum_m \sum_n B_{mn}\psi_{mn}(x,y) \tag{2.20}$$

Multiplying both sides of (2.20) by $\psi_{m'n'}(x,y)$, integrating over the patch surface and using the orthonormality condition of ψ_{mn}, B_{mn} can be obtained as

$$B_{mn} = \psi_{mn}(x_p, y_p). \tag{2.21}$$

Substituting (2.21) into (2.20), and substituting the resulting expression for the impulse function and (2.19) into (2.18), one can obtain the following equality:

$$\sum_m \sum_n A_{mn}(k^2 - k_{mn}{}^2)\psi_{mn}(x,y) = \sum_m \sum_n \psi_{mn}(x_p, y_p)\psi_{mn}(x,y) \tag{2.22}$$

which results in

$$A_{mn} = \frac{\psi_{mn}(x_p, y_p)}{k^2 - k_{mn}{}^2}. \tag{2.23}$$

As a result, the Green's function G_z is obtained as

$$G_z(x, y; x_p, y_p) = \sum_m \sum_n \frac{\psi_{mn}(x_p, y_p)\psi_{mn}(x,y)}{k^2 - k_{mn}^2}. \tag{2.24}$$

After having obtained the Green's function, the excitation needs to be modelled mathematically to be able to perform the convolution operation. So, the coaxial feed is idealized by a uniform z-directed current sheet, lying either along x-direction or along y-direction. For the current sheet lying along x-direction, the current distribution on the probe is assumed to be

$$\mathbf{J} = \hat{\mathbf{z}} \frac{\tilde{\delta}(y - y_p)}{d}\left[U\left(x - x_p + \frac{d}{2}\right) - U\left(x - x_p - \frac{d}{2}\right)\right] \tag{2.25}$$

and for the one lying along y-direction, it is

$$\mathbf{J} = \hat{\mathbf{z}} \frac{\tilde{\delta}(x - x_p)}{d}\left[U\left(y - y_p + \frac{d}{2}\right) - U\left(y - y_p - \frac{d}{2}\right)\right] \tag{2.26}$$

where U is the unit step function, d is the effective width of the current sheet, and the current distribution corresponds to a feed current of one ampere. Although this choice of the current distribution is somewhat arbitrary, it gives good agreement between experimental results and theoretical calculations of the impedance loci of

various antennas [21].

Now, since we are equipped with the Green's function and the analytical representation of the source, the actual electric field distribution inside the cavity can be determined by the convolution integral of this extended source and the Green's function:

$$E_z(x,y) = j\omega\mu \iint dx'dy' G_z(x,y;x',y') J(x',y') \tag{2.27}$$

which results in

$$E_z(x,y) = j\omega\mu \sum_m \sum_n \frac{\psi_{mn}(x,y)\psi_{mn}(x_p,y_p)}{k^2 - k_{mn}^2} \operatorname{sinc}\left(\frac{md}{2a}\right) \tag{2.28}$$

for the current sheet lying along x-direction, and

$$E_z(x,y) = j\omega\mu \sum_m \sum_n \frac{\psi_{mn}(x,y)\psi_{mn}(x_p,y_p)}{k^2 - k_{mn}^2} \operatorname{sinc}\left(\frac{nd}{2b}\right) \tag{2.29}$$

for the one lying along y-direction.

Although the cavity model accurately predicts the shape of the internal fields, the amplitude of the field, namely the coefficients C_{mn} in (2.8), differs greatly for the cavity and the radiating antenna.

At resonance, the real parts of k^2 and k_{mn}^2 cancel each other and only $-j\omega^2\mu\varepsilon\delta$ term remains in the denominator of (2.28) and (2.29). Therefore, the magnitudes of the internal fields are mainly dependent on δ, which is the loss tangent accounting only for dielectric losses. Using a modified loss tangent δ_{eff}

$$\delta_{eff} = \frac{1}{Q} \tag{2.30}$$

which accounts for the loss of power in radiation and through heating of the conductor cladding, the accurate magnitude of the electric field can be determined [21]. With this modified loss tangent, the power lost by the antenna is

redistributed throughout the field.

Once the electric field is calculated, the magnetic field in the cavity can be derived from (2.2) and (2.28) for the current sheet lying along x-direction,

$$\mathbf{H} = j\frac{\nabla \times \mathbf{E}_z}{\omega\mu} = \mathbf{x}H_x + \mathbf{y}H_y \tag{2.31}$$

where

$$H_x = -j\omega\mu \sum_m \sum_n \frac{\psi_{mn}(x_p, y_p)\alpha_{mn}}{k^2 - k_{mn}^2}\left(\frac{n\pi}{b}\right)\cos\left(\frac{m\pi x}{a}\right)\sin\left(\frac{n\pi y}{b}\right)\mathrm{sinc}\left(\frac{md}{2a}\right) \tag{2.32}$$

$$H_y = -j\omega\mu \sum_m \sum_n \frac{\psi_{mn}(x_p, y_p)\alpha_{mn}}{k^2 - k_{mn}^2}\left(\frac{m\pi}{a}\right)\cos\left(\frac{n\pi y}{b}\right)\sin\left(\frac{m\pi x}{a}\right)\mathrm{sinc}\left(\frac{md}{2a}\right) \tag{2.33}$$

For the source lying along y-direction,

$$H_x = -j\omega\mu \sum_m \sum_n \frac{\psi_{mn}(x_p, y_p)\alpha_{mn}}{k^2 - k_{mn}^2}\left(\frac{n\pi}{b}\right)\cos\left(\frac{m\pi x}{a}\right)\sin\left(\frac{n\pi y}{b}\right)\mathrm{sinc}\left(\frac{nd}{2b}\right) \tag{2.34}$$

$$H_y = -j\omega\mu \sum_m \sum_n \frac{\psi_{mn}(x_p, y_p)\alpha_{mn}}{k^2 - k_{mn}^2}\left(\frac{m\pi}{a}\right)\cos\left(\frac{n\pi y}{b}\right)\sin\left(\frac{m\pi x}{a}\right)\mathrm{sinc}\left(\frac{nd}{2b}\right) \tag{2.35}$$

From the above field expressions, one can observe that a specific mode is excited if the excitation current has a frequency near the resonant frequency of that particular mode, and if it is properly located. Placing the probe feed, with an impressed current density **J**, to the nodal line ($E_z = 0$) of a particular mode cannot excite that mode, whereas the strongest coupling to the antenna for that mode is obtained when the probe is placed to the position where the electric field E_z is maximum for the mode. This fact brings out an important intuition on the input impedance, which is: if the feed is positioned where the electric field is maximum then the input impedance becomes maximum; when positioned where the electric field is minimum then the input impedance becomes minimum. Using this

observation, one can match the input impedance to any impedance value without using additional circuitry.

2.2.2 Derivation of Far-Zone Fields

To find the radiation from microstrip antennas, two different approaches can be used [55]:

- Electric Current Model
- Magnetic Current Model

In this thesis, magnetic current model with truncated substrate structure is used. This model primarily applies the equivalence principle at the boundary S shown in Fig. 2.5.

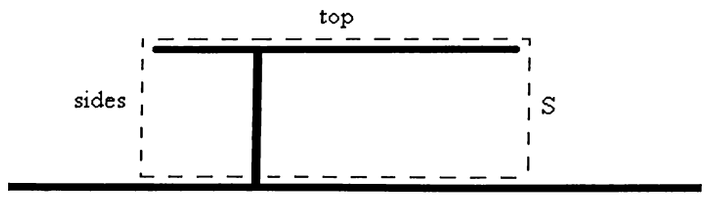

Figure 2.5: Application of equivalence principle to microstrip antennas (side view)

Since the dielectric substrate is thin, this model neglects its effect on the far field radiation and replaces the interior of S with air. It also assumes zero fields inside S, because the region of interest for the radiated fields is outside of the cavity. Consequently, the resulting electric and magnetic current densities to satisfy these conditions on the boundary S are found to be:

$$\mathbf{J}_s = \hat{\mathbf{n}} \times \mathbf{H} = \mathbf{J}_s^{up} \approx 0 \tag{2.36}$$

$$\mathbf{M}_s = -\hat{\mathbf{n}} \times \mathbf{E} = 0 \text{ (due to PEC)} \tag{2.37}$$

on the top,

$$\mathbf{J}_s = \hat{\mathbf{n}} \times \mathbf{H} \approx 0 \tag{2.38}$$

$$\mathbf{M}_s = -\hat{\mathbf{n}} \times \mathbf{E} \text{ (due to PMC)} \tag{2.39}$$

on the sides, where $\hat{\mathbf{n}}$ is the unit vector normal to S and pointing outwards, and $\mathbf{J}_s^{up}$ refers to the electric current density at $z = h+0$, which is the upper side of the patch. Since the internal fields are very large near the resonant frequency, the electric current density at the lower side *(at $z = h-0$)* of the patch dominates:

$$\left|J_s^{low}\right| >> \left|J_s^{up}\right| \tag{2.40}$$

therefore, $\mathbf{J}_s^{up}$ is assumed to be negligible.

Accounting the image in the ground plane, the resulting magnetic current density lying along the patch periphery is

$$\mathbf{M}_s = -2\hat{\mathbf{n}} \times \hat{\mathbf{z}} E_z \tag{2.41}$$

with the following properties:

- The magnetic current M of the *(m,n)*th mode has m zeros along x side and n zeros along y side.
- The distance between the two adjacent zeros is $\lambda_\varepsilon/2$ where $\lambda_\varepsilon = \dfrac{\lambda_0}{\sqrt{\varepsilon_r}}$.
- M reverses direction whenever it crosses a zero.
- M is a continuous function, sinusoidal or constant, around the perimeter of the patch.

The far-zone fields can be calculated by [56],

$$\mathbf{E}(\mathbf{r}) = \frac{j\omega\mu e^{-jk_0 r}}{4\pi r \eta_0} \mathbf{r} \times \iint ds' e^{jk_0 \mathbf{r}\cdot\mathbf{r}'} \mathbf{M}_s(\mathbf{r}') \tag{2.42}$$

where $\eta_0 = \sqrt{\frac{\mu}{\varepsilon_0}}$, $\mathbf{r} = \hat{\mathbf{x}}x + \hat{\mathbf{y}}y + \hat{\mathbf{z}}z$, and $(')$ corresponds to source locations.

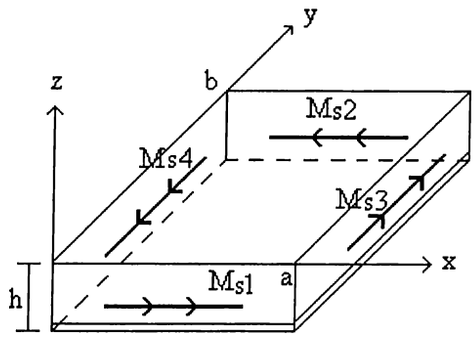

Figure 2.6: Magnetic current sources along the patch periphery

As shown in Figure 2.6, the total surface magnetic current density along the patch periphery is written as

$$\begin{aligned}\mathbf{M}_s &= \mathbf{M}_{s1} + \mathbf{M}_{s2} + \mathbf{M}_{s3} + \mathbf{M}_{s4} \\ &= \hat{\mathbf{x}}2[E_z(x,0) - E_z(x,b)][U(x) - U(x-a)] \\ &\quad + \hat{\mathbf{y}}2[E_z(a,y) - E_z(0,y)][U(y) - U(y-b)]\end{aligned} \tag{2.43}$$

and by substituting (2.43) into (2.42), the radiated electric field is obtained from

$$\begin{aligned}\mathbf{E}(\mathbf{r}) = \frac{j\omega\mu e^{-jk_0 r}}{4\pi r\eta} 2\mathbf{r} \times \{ &\hat{\mathbf{x}}\int_0^h dz \int_0^a dx E_z(x,0) e^{jk_0 \hat{\mathbf{r}}\cdot(\hat{\mathbf{x}}x + \hat{\mathbf{z}}z)} \\ &- \hat{\mathbf{x}}\int_0^h dz \int_0^a dx E_z(x,b) e^{jk_0 \hat{\mathbf{r}}\cdot(\hat{\mathbf{x}}x + \hat{\mathbf{y}}b + \hat{\mathbf{z}}z)} - \hat{\mathbf{y}}\int_0^h dz \int_0^h dy E_z(0,y) e^{jk_0 \hat{\mathbf{r}}\cdot(\hat{\mathbf{y}}y + \hat{\mathbf{z}}z)} \\ &+ \hat{\mathbf{y}}\int_0^h dz \int_0^h dy E_z(a,y) e^{jk_0 \hat{\mathbf{r}}\cdot(\hat{\mathbf{x}}a + \hat{\mathbf{y}}y + \hat{\mathbf{z}}z)} \}\end{aligned} \tag{2.44}$$

The spherical-coordinate representations of $\hat{\mathbf{x}}$, $\hat{\mathbf{y}}$ and $\hat{\mathbf{z}}$ are used to represent the field components in the spherical coordinates. For the sake of completeness, they

are given here as

$$\begin{aligned}\hat{\mathbf{x}} &= \hat{\mathbf{r}}\sin\theta\cos\phi + \hat{\boldsymbol{\theta}}\cos\theta\cos\phi - \hat{\boldsymbol{\phi}}\sin\phi \\ \hat{\mathbf{y}} &= \hat{\mathbf{r}}\sin\theta\sin\phi + \hat{\boldsymbol{\theta}}\cos\theta\sin\phi + \hat{\boldsymbol{\phi}}\cos\phi \\ \hat{\mathbf{z}} &= \hat{\mathbf{r}}\cos\theta - \hat{\boldsymbol{\theta}}\sin\theta\end{aligned} \tag{2.45}$$

Using these representations in (2.44), the final expression for **E(r)** is obtained as

$$\mathbf{E}(r) = \sum_m \sum_n \left(\hat{\boldsymbol{\phi}} E_\phi^{\,mn}(r) + \hat{\boldsymbol{\theta}} E_\theta^{\,mn}(r)\right) \tag{2.46}$$

where

$$E_\phi^{mn}(r) = \frac{-j\omega\mu 2he^{-jk_0 r}\alpha_{mn}}{\pi r\left(k^2 - k_{mn}^2\right)}\psi_{mn}(x_p, y_p)\operatorname{sinc}\left(\frac{md}{2a}\right)k_{z0}e^{j\left(\frac{a}{2}k_{x0}+\frac{b}{2}k_{y0}\right)} \tag{2.47}$$

$$(-j)^{m+n}\sin\left(\frac{k_{y0}b}{2}-\frac{n\pi}{2}\right)\sin\left(\frac{k_{x0}a}{2}-\frac{m\pi}{2}\right)\left\{\frac{k_{x0}\cos\phi}{\left(\frac{m\pi}{a}\right)^2 - k_{x0}^{\,2}} - \frac{k_{y0}\sin\phi}{\left(\frac{n\pi}{b}\right)^2 - k_{y0}^{\,2}}\right\}$$

and

$$E_\phi^{mn}(r) = \frac{-j\omega\mu 2he^{-jk_0 r}\alpha_{mn}}{\pi r\left(k^2 - k_{mn}^2\right)}\psi_{mn}(x_p, y_p)\operatorname{sinc}\left(\frac{md}{2a}\right)k_{x0}e^{j\left(\frac{a}{2}k_{x0}+\frac{b}{2}k_{y0}\right)} \tag{2.48}$$

$$(-j)^{m+n}\sin\left(\frac{k_{y0}b}{2}-\frac{n\pi}{2}\right)\sin\left(\frac{k_{x0}a}{2}-\frac{m\pi}{2}\right)\left\{\frac{k_0\sin\phi}{\left(\frac{m\pi}{a}\right)^2 - k_{x0}^{\,2}} + \frac{k_0\sin\phi}{\left(\frac{n\pi}{b}\right)^2 - k_{y0}^{\,2}}\right\}$$

with

$$\begin{aligned}k_{z0} &= k_0\cos\theta \\ k_{x0} &= k_0\sin\theta\cos\phi \\ k_{y0} &= k_0\sin\theta\sin\phi\end{aligned} \tag{2.49}$$

for the source lying along x-direction. The far-zone fields due to a source lying

along y-direction are the same, with a minor difference that all $\text{sinc}\left(\frac{md}{2a}\right)$ terms are replaced with $\text{sinc}\left(\frac{nd}{2b}\right)$.

2.2.3 Quality Factor Calculation

The quality factor, or Q, of a resonator is defined as [57]

$$Q = 2\pi \frac{\textbf{time - average energy stored at a resonant frequency}}{\textbf{energy dissipated in one period of this frequency}} \tag{2.50}$$

$$= \omega \frac{W_e + W_m}{P_r + P_d + P_c}$$

where, for the rectangular patch shown in Figure 2.4,

$$W_e = \frac{\varepsilon_0 \varepsilon_r h}{4} \int_0^b \int_0^a \mathbf{E}_z . \mathbf{E}_z^* dxdy \tag{2.51}$$

= average stored energy in the electric field,

$$W_m = \frac{\mu h}{4} \int_0^b \int_0^a \mathbf{H}.\mathbf{H}^* dxdy$$

= average stored energy in the magnetic field, (2.52)

$$P_r = \frac{1}{2\eta_0} \int_0^{2\pi} \int_0^{\pi/2} \left(|E_\theta|^2 + |E_\phi|^2 \right)^2 \sin\theta d\theta d\phi \tag{2.53}$$

= total radiated power,

$$P_d = 2\omega\delta W_e \tag{2.54}$$

= power dissipated due to dielectric losses,

$$P_c = \frac{2\omega\Delta W_m}{h} \tag{2.55}$$

= power dissipated due to conductor losses (patch + ground),

δ = loss tangent of the substrate,

$$\Delta = \sqrt{\frac{2}{\omega\mu\sigma}} \tag{2.56}$$

= skin depth of the patch and ground plane,

σ = conductivity.

The Q-factor can also be expressed by

$$\frac{1}{Q} = \frac{1}{Q_d} + \frac{1}{Q_r} + \frac{1}{Q_c} \tag{2.57}$$

where

$$Q_d = \frac{1}{\delta} \tag{2.58}$$

= Q-factor of dielectric loss,

$$Q_c = \frac{h}{\Delta} \tag{2.59}$$

= Q-factor of conductor loss,

$$Q_r = \frac{2\omega W_e}{P_r} \tag{2.60}$$

= Q factor of radiation loss.

If the dielectric in the cavity (with perfectly conducting electric and magnetic walls) is assumed to have a dielectric loss tangent of $1/Q$, Eq. (2.57), the loss of power in radiation and through heating of the conductor cladding is accounted and the cavity behaves like the antenna. The most dominant contribution, hopefully, to this quality factor is from the radiation of the antenna. However, for thin microsrip antennas, Q_r is considerably less than Q_d and Q_c, which is the main reason for the narrow bandwidth of thin microstrip antennas.

2.2.4 Calculation of Input Impedance

If the dielectric material and the metal parts within the cavity were assumed to be lossless, then the analysis of the cavity would yield purely reactive input impedance. However, the input impedance of the corresponding microstrip antenna can not be purely reactive, because its resistive part accounts for the power radiated by the antenna.

With a view of this argument, the input impedance expression for the ideal cavity has only real poles of frequency, while that of the corresponding antenna has complex poles of frequency. The imaginary parts of these poles account for the power lost by radiation and by dielectric and conduction losses. The real parts of the corresponding cavity and antenna poles are dependent on the shapes of their modal field distributions and are consequently almost identical for thin elements. To make the cavity more resemble the antenna it is supposed to model, one can add loss to the cavity dielectric (in the analysis) by appropriately adjusting the loss tangent of the cavity dielectric. The imaginary parts of the poles of the cavity filled with the lossy dielectric will no longer be zero.

There are several ways to calculate the input impedance of a microstrip antenna, but in this thesis, we present two of them, both of which give the same result; one uses the expression for the input power, and the other calculates the voltage/current ratio at the feed point.

(i) Derivation of Input Impedance from Input Power

Power supplied by the external source J is given by

$$P = -\int_{v} \mathbf{E}.\mathbf{J}^{*} dv \tag{2.61}$$

$$= VI^*$$
$$= Z_{in} II^*$$

which implies that

$$Z_{in} = \frac{P}{|I|^2} \tag{2.62}$$

where the input current is assumed to be *1* Amp. For a current sheet lying along *x*-direction, using vectors **J** and $\mathbf{E_z}$ given in (2.25) and (2.28), respectively, the expression for Z_{in} is obtained as

$$Z_{in} = -j\omega\mu h \sum_m \sum_n \frac{\psi_{mn}^2(x_p, y_p)}{k^2 - k_{mn}^2} \text{sinc}^2\left(\frac{md}{2a}\right) \tag{2.63}$$

For a source lying along *y*-direction, using vectors **J** and $\mathbf{E_z}$ that are given in (2.26) and (2.29), respectively, the input impedance Z_{in} is obtained as

$$Z_{in} = -j\omega\mu h \sum_m \sum_n \frac{\psi_{mn}^2(x_p, y_p)}{k^2 - k_{mn}^2} \text{sinc}^2\left(\frac{nd}{2b}\right) \tag{2.64}$$

(ii) Derivation of Input Impedance From Input Voltage

The definition of the input impedance at the port where the voltage and current is well defined is written as

$$Z_{in} = \frac{V_{in}}{I} \tag{2.65}$$

where V_{in} is the driving point voltage and I is the source current. Since the electric field inside the patch is z-directed and independent of z, V_{in} can be directly written as

$$V_{in} = -hE_z \tag{2.66}$$

This voltage needs to be averaged over the width of the feeding strip to take the finite size of the feed into consideration. For a z-polarized current source lying along x-direction, with amplitude of 1 Amp, the input impedance can be obtained from

$$Z_{in} = -\frac{h}{d}\left(\int_{x-d/2}^{x+d/2} E_z dx\right)\Bigg|_{\substack{x=x_p \\ y=y_p}} \tag{2.67}$$

where $\mathbf{E_z}$ is given in (2.28), and the same result as in (2.63) is obtained. For the same source, but now lying along y-direction, the input impedance is obtained from

$$Z_{in} = -\frac{h}{d}\left(\int_{y-d/2}^{y+d/2} E_z dy\right)\Bigg|_{\substack{x=x_p \\ y=y_p}} \tag{2.68}$$

which results in the same expression as in (2.64) with the use of $\mathbf{E_z}$ in (2.29).

2.2.5 Determination of Resonant Frequency

There are a number of different theories available for computing the resonant frequency of a microstrip element. One of the simplest, though not the most accurate, is that provided by the Cavity Model. In the Cavity Model, the resonant frequency of each mode is calculated by

$$f_{mn} = k_{mn}\frac{c_0}{2\pi\sqrt{\varepsilon_r}} \tag{2.69}$$

where $k_{mn} = \sqrt{\left(\frac{m\pi}{a}\right)^2 + \left(\frac{n\pi}{b}\right)^2}$. This is due to the assumption that the field under

the microstrip antenna is distributed in about the same way as the field in the corresponding magnetic-walled cavity. However, this formula does not include the effect of all modes, hence does not consider the stored energy in other modes. If this equation is used, with no modification on the dimensions of the patch to account for the fringing fields, to predict the resonant frequency, the accuracy of the results would be quite low, of course depending upon the particular shape of the patch, mode being used and the thickness of the substrate.

The resonance frequency of an antenna can be defined in two ways:

1. The frequency, at which the voltage standing wave ratio (*VSWR*), referred to the input terminals of the antenna, is minimum. This is also equal to the frequency, at which the reflection coefficient has minimum magnitude.
2. The frequency, at which the input impedance Z_{in}, referred to the input terminals, has maximum resistance value independent of the value of reactance.

In this thesis, the minimum magnitude of the reflection coefficient is used in determining the resonant frequency of rectangular patches. The reflection coefficient is determined from the input impedance by

$$\Gamma_{in} = \frac{Z_{in} - Z_0}{Z_{in} + Z_0} \tag{2.70}$$

where Z_0 is chosen as 50Ω. With the use of the input impedance, which includes the effect of the other modes into account, the stored energy in all modes is also taken into consideration.

From the earlier discussion of the cavity approximation of the microstrip

antennas, it is acknowledged that the use of the PMC walls for the openings around the microstrip antenna is just an approximation, and cannot provide exactly the same field distribution at the edges of the antenna. This is mainly due to the normal component of the electric field at the periphery of the antenna that cannot be represented by the cavity model, and usually referred to as fringing fields. This is because normal electric fields at PMCs must be equal to zero, and according to the cavity model all side walls of the cavity are made of PMCs. To compensate this in the simulations of microstrip antennas via the cavity model, the effective dimensions of the patch are determined using the extensions to each dimension of the antenna, as given in Appendix A, that accounts for the fringing fields. In other words, the fringing fields at the edges are accounted for by extending the patch boundary outwards and considering the effective dimensions to be somewhat larger than the physical dimensions of the patch [46]. The resonant frequencies are calculated for various probe-fed rectangular patches and compared with the results given in Kara's paper [58]. The results are tabulated in Table 2.1, where Δ is the % deviation and defined as

$$\Delta = 100\frac{f_{r-cavity} - f_{r-paper}}{f_{r-paper}} \tag{2.71}$$

In the simulations given in the table, the effective width of the probe feed, d, is taken as 1 mm, and the patches are fed from the middle of side a, namely $x_p = a/2$. In addition, conductivity of the patch and the ground plane is chosen as 5.8×10^5 mho/cm, which is the conductivity of copper.

The resonant frequencies calculated using the cavity model agree well with the measured results, with a slight deviation within the tolerable range. From these

results, it is concluded and verified that the cavity model for the determination of the resonant frequency is very accurate for thin antennas, as expected, and its accuracy deteriorates as the thickness of the substrate increases.

Table 2.1: Resonant frequencies for various antennas. Dimensions are in cm, frequencies are in GHz.

a	b	h	ε_r	y_p	δ	$f_{r\text{-paper}}$	$f_{r\text{-cavity}}$	$\%\Delta$
0.85	1.29	0.017	2.22	0.415	0.001	7.74	7.695	0.58
0.79	1.185	0.017	2.22	0.41	0.001	8.45	8.37	0.95
2	2.5	0.079	2.22	0.683	0.001	3.97	3.94	0.76
1.063	1.183	0.079	2.22	0.39	0.001	7.73	8.195	-6.02
0.91	1	0.127	10.2	0.375	0.001	4.6	4.38	4.78
1.72	1.86	0.157	2.33	0.594	0.001	5.06	5.06	0.0
1.81	1.96	0.157	2.33	0.627	0.001	4.805	4.81	-0.1
1.27	1.35	0.163	2.55	0.425	0.002	6.56	6.545	0.23
1.5	1.621	0.163	2.55	0.528	0.002	5.6	5.515	1.52
1.337	1.412	0.2	2.55	0.475	0.002	6.2	6.175	0.4
1.12	1.2	0.242	2.55	0.425	0.002	7.05	7.01	0.57
1.403	1.485	0.252	2.55	0.46	0.002	5.8	5.77	0.52
1.53	1.63	0.3	2.50	0.47	0.002	5.27	5.245	0.47
1.17	1.28	0.3	2.50	0.37	0.002	6.57	6.495	1.14
0.905	1.018	0.3	2.50	0.34	0.002	7.99	7.84	1.88
1.375	1.58	0.476	2.55	0.882	0.002	5.1	4.99	2.16

Chapter 3

Dual Frequency Operation and Multi-port Analysis

Many communication systems often require dual-band operation where the same antenna can be used as a transmitter and/or receiver at two distinct frequencies. This is especially witnessed in cellular communications, which have experienced enormous growth over the last decade. The frequency bands allocated for the wireless communication in Europe are 890-960 MHz for the GSM (Global System for Mobile) band and 1710-1880 MHz for the DCS-1800 (Digital Communication System-1800) band. Since there are two different frequency bands allocated, subscribers who travel over service areas employing different frequency bands need two separate antennas unless a dual-frequency antenna is used. Because of this, recently, there has been considerable interest in the development of dual-band microstrip antennas.

Several methods for obtaining dual-band operation have been developed, such as stacked microstrip antennas, slotted microstrip antennas, loading the patch with reactive stubs or with shorting pins, etc. In this chapter, general information on dual-frequency operation of single-element microstrip antennas is first discussed, and then a detailed study on multi-port analysis of microstrip antennas with shorting pins is provided.

3.1 Dual Frequency Operation of Single Element Microstrip Antennas

Dual frequency operation using a single element is advantageous in terms of saving space, using less material, preventing undesirable grating lobes due to the large element spacing for the high band and design simplicity.

The Cavity Model approach, presented in Chapter 2, proves that a single rectangular patch antenna can be excited for multimode operation, that is, it can operate on different modes with different resonant frequencies. To make this dual frequency operation useful, the following restrictions are imposed on the two bands:

- Same radiation pattern,
- Same polarization,
- Same input impedance,
- A desired frequency ratio.

It is obvious that these restrictions make many cavity modes useless. As the difference between the two frequencies increases, the radiation patterns do not remain the same for both of the bands. In addition, as the frequency difference increases, the patch dimensions that are suitable for the low mode turn to be too large for the high mode. This results in grating lobes in the radiation pattern and cross polarization. Therefore, the lowest modes should be chosen to have small frequency difference. The two lowest TM modes are (0,1) and (1,0) modes, but they have different polarizations.

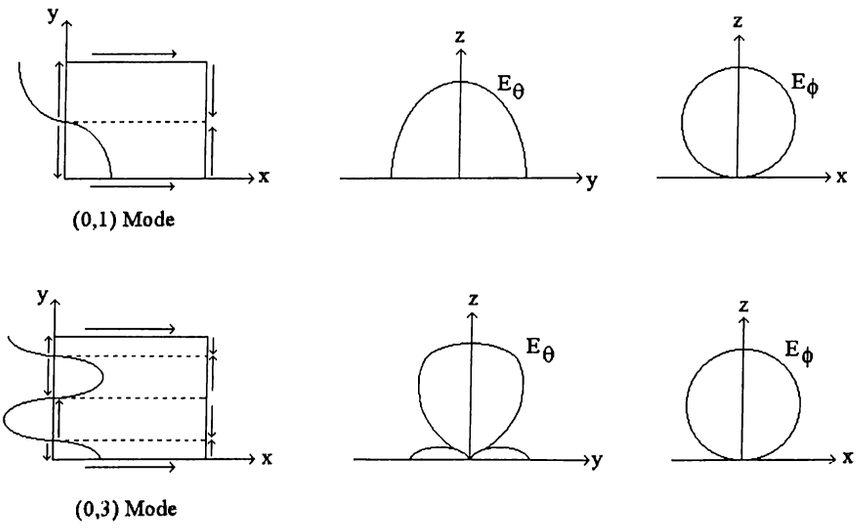

Figure 3.1: Edge magnetic current distributions and radiation pattern sketches of (0,1) and (0,3) modes.

Therefore, the two lowest useful TM modes are (0,1) and (0,3) modes, both of which have broadside radiation patterns, same polarizations and similar input impedances. The magnetic current distributions at the edges and the radiation patterns of these two modes are given in Figure 3.1. Both of these modes are linearly polarized in the same direction and have a fixed frequency ratio f_{03}/f_{01} of approximately 3. Note that the exact ratio depends on the

fringing fields. To adjust this ratio, some methods have been developed and implemented successfully, which are

- Placing shorting pins between the patch and ground plane,
- Cutting slots in the patch.

Both methods are aimed to decrease f_{03}/f_{01} ratio. Shorting pins achieve this by increasing f_{01} and slots by decreasing f_{03}.

Since both the low and high band operations lack modal purity, it is better to use f_l instead of f_{01}, and f_h instead of f_{03}. For the sake of illustration, a typical probe-fed rectangular patch with both slot and shorting strip is shown in Figure 3.2.

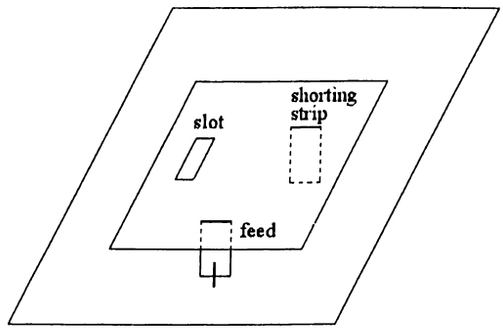

Figure 3.2: Rectangular probe-fed patch with both slot and shorting strip.

To reduce f_h / f_l ratio, shorting pins are placed on the nodal line ($E_z = 0$) of the (0,3) mode, so that they practically do not affect the field distribution of this modal field; hence its resonant frequency remains unaffected. In addition to the placement of the shorting pins along the nodal line of (0,3) mode, their positions are also dependent on the amount of shift in the resonant frequency of the (0,1) mode that is required to satisfy a pre-defined ratio. In other words, the field distribution of the (0,1) modal field in the cavity is changed, with the

help of the shorting pins, to make it look like it is the field distribution of the required f_l. With a view of this, the resonant frequency of the modified mode can be tuned over a wide range, independent of the high band. This approach gives a great deal of design flexibility, and it was demonstrated that f_h/f_l can be changed from 3.04 to 2.09 using maximum six pins by Lo *et al.* [21]. The positions of the pins and feed are shown in Figure 3.3, and the effect of placing pins is demonstrated in Table 3.1.

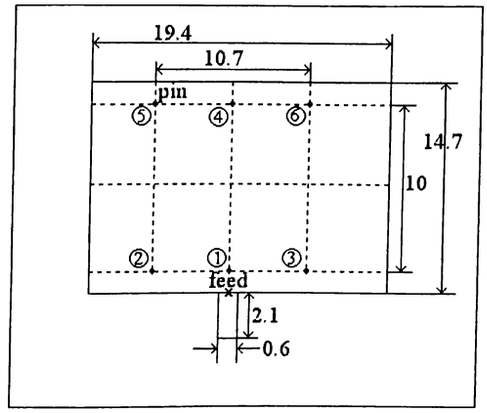

Figure 3.3: The geometry of rectangular patch with shorting pins. All dimensions are in cm, h = 0.316 cm, $\varepsilon_r = 2.62$, $\delta = 0.001$, $\sigma = 270$ Kmho/cm.

Pin number	Pin Position	f_l(MHz)	f_h(MHz)	f_h/f_l
0	-	613	1861	3.04
1	1	664	1864	2.82
2	1,2	706	1865	2.64
3	1,2,3	792	1865	2.36
4	1,2,3,6	813	1865	2.29
5	1,2,3,5,6	846	1865	2.20
6	1,2,3,4,5,6	891	1865	2.09

Table 3.1: The effect of shorting pins on the resonant frequencies

It is observed that the effect of pin tuning diminishes after a number of pins have been inserted. To reduce f_h/f_l further, slots can be cut in the patch, where the magnetic field of the (0,3) mode is maximum. These slots affect the (0,3) modal field drastically, and reduce its resonant frequency, but do not change the (0,1) modal field, hence its resonant frequency. This way, the resonant frequency of (0,3) mode can be lowered. Wang and Lo [43] have shown that by using three slots and 10 pins maximum, the effect of pin and slot tuning diminishes, and f_h/f_l can be reduced to about 1.3. The feed, pin and slot positions, and the corresponding results are shown in Figure 3.4 and Table 3.2, respectively. Again, it is observed that the effect of slots for tuning the resonant frequency diminishes after a certain number of slots.

In this thesis, dual-frequency operation of rectangular probe-fed patch antennas using shorting pins is investigated. For the analysis of microstrip antennas with shorting pins, Richards and Lo [59] developed a CM-based approach, called multi-port analysis, which is presented in the following section in details.

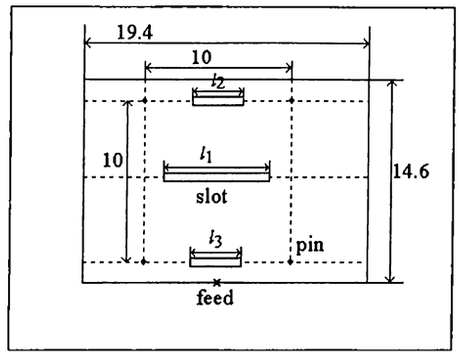

Figure 3.4: The geometry of rectangular patch with slots and shorting pins. All dimensions are in cm, h = 0.158 cm, $\varepsilon_r = 2.62$, $\delta = 0.001$, $\sigma = 270$ Kmho/cm.

Case	Description (dimensions are in cm)	f_l(MHz)	f_h(MHz)	f_h/f_l
1	One slot l_1=1.0 at (9.7, 7.3)	628	1900	3.02
2	One slot l_1=4.5 at (9.7, 7.3)	596	1700	2.85
3	Three slots l_1=7.0 cm, l_2=l_3=3.0 at (9.7, 2.4), (9.7, 7.3), and (9.7, 12.2)	555	1420	2.55
4	Three slots l_1=l_2=l_3=7.0 at the same locations as in case 3	553	1310	2.36
5	Same as case 4, but with four pins as shown in Figure 3.4	698	1087	1.56
6	Same as case 5 with six additional pins at (3.7, 2.4), (9.7, 2.4), (15.7, 2.4), (3.7, 12.2), (9.7, 12.2), (15.7, 12.2)	890	1181	1.31

Table 3.2: The effect of slots and shorting pins on the resonant frequencies

3.2 Multi-port Analysis of Microstrip Antennas with Shorting Pins

For the application of the multi-port analysis, the underlying assumption is that the system is linear and the superposition principle can be applied. This is true for the microstrip antennas, but before getting into the details of the application of this approach for microstrip antennas, it would be instructive first to review the multi-port analysis of an N port system, as shown in Figure 3.5. The relation between the port voltages and port currents is given with the following current controlled representation:

$$\begin{bmatrix} V_1 \\ V_2 \\ \vdots \\ V_N \end{bmatrix} = \begin{bmatrix} Z_{11} & Z_{12} & \cdots & Z_{1N} \\ Z_{21} & Z_{22} & \cdots & Z_{2N} \\ \vdots & \vdots & \vdots & \vdots \\ Z_{N1} & Z_{N2} & \cdots & Z_{NN} \end{bmatrix} \begin{bmatrix} I_1 \\ I_2 \\ \vdots \\ I_N \end{bmatrix} \tag{3.1}$$

where $V_i = \sum_{j=1}^{N} Z_{ij} I_j$ for $i, j=1,...,N$ and $Z_{ij} = Z_{ji}$. The mutual impedance Z_{ij} is by definition the open circuit voltage at the i^{th} port due to a unit current at the j^{th} port with all other ports open:

$$Z_{ij} = \left[V_i / I_j\right]_{I_i=0} \qquad for\ all\ i's \neq j \tag{3.2}$$

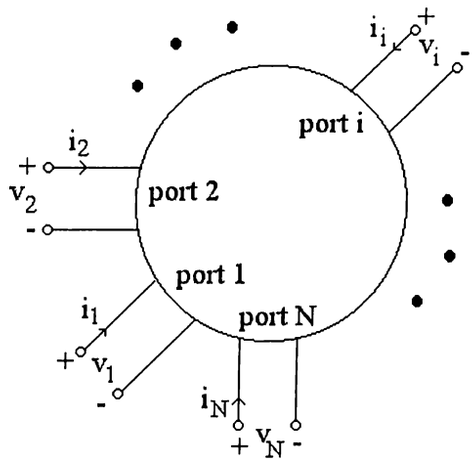

Figure 3.5: N port system with the corresponding port voltages and port currents.

From these open-circuit or *Z*-parameters, one can compute the corresponding *S*-parameters of the system by

$$S = (ZY_0 + I)^{-1}(ZY_0 - I) \tag{3.3}$$

where I is the unit matrix and Y_0 is the diagonal matrix containing the characteristic admittances of the feed lines to the ports.

In the multi-port analysis of microstrip antennas with shorting pins, the feed position is considered as the first port and the shorting pins are considered

as additional ports, namely as current sources. To find the input impedance at the feed port, all other ports are short-circuited, that is, zero voltages are applied to the shorting-pin ports. To make things clear, consider the rectangular patch with a feed point of coordinates (x_1, y_1) and a shorting pin of coordinates (x_2, y_2) as shown in Figure 3.6. Let d_1 be the effective width of the feed and d_2 be the effective width of the pin.

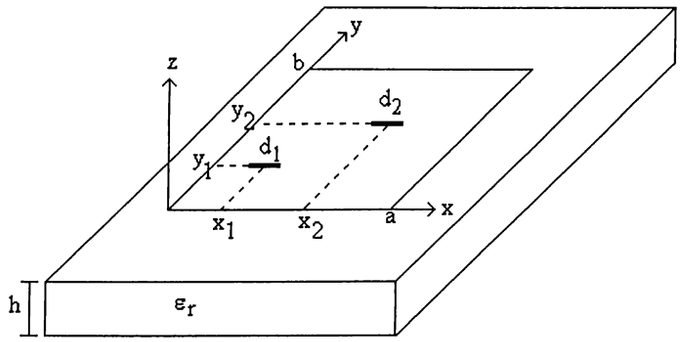

Figure 3.6: Geometry of microstrip antenna with one x-directed probe feed and one x-directed shorting pin.

Using the Z-matrix representation of the system, the port voltages are related to the port currents as

$$\begin{bmatrix} V_1 \\ V_2 \end{bmatrix} = \begin{bmatrix} Z_{11} & Z_{12} \\ Z_{21} & Z_{22} \end{bmatrix} \begin{bmatrix} I_1 \\ I_2 \end{bmatrix}. \tag{3.4}$$

The input impedance at the feed port, when the second port is short circuited, is calculated by assigning $V_2 = 0$ in the above matrix equation:

$$V_1 = Z_{11} I_1 + Z_{12} I_2 \tag{3.5}$$

$$V_2 = Z_{21} I_1 + Z_{22} I_2 = 0 \tag{3.6}$$

$$Z_{in} = \frac{V_1}{I_1} = Z_{11} - \frac{Z_{12}^2}{Z_{22}} \tag{3.7}$$

where the mutual impedances, Z_{ij}'s, can be determined using the cavity model. The mutual impedances, Z_{ij}'s, are calculated by averaging the voltage created by the i^{th} source over the j^{th} source. For the input current I located at point (x_i,y_i), the electric field E_{zi} anywhere under the patch has been given in Chapter 2 as

$$E_{zi} = -j\omega\mu \sum_m \sum_n \frac{\psi_{mn}(x,y)\psi_{mn}(x_i,y_i)}{k^2 - k_{mn}^2} \operatorname{sinc}\left(\frac{md_i}{2a}\right) \tag{3.8}$$

then, the voltage created by i^{th} source is written as

$$V_i = -hE_{zi} \quad . \tag{3.9}$$

Using z-polarized current distributions along the two strips lying in x-direction, J_{zi} and J_{zj} for strips i and j, respectively,

$$J_{zi} = \frac{\tilde{\delta}(y - y_i)}{d_i}\left[U\left(x - x_i + \frac{d_i}{2}\right) - U\left(x - x_i - \frac{d_i}{2}\right)\right] \tag{3.10}$$

$$J_{zj} = \frac{\tilde{\delta}(y - y_j)}{d_j}\left[U\left(x - x_j + \frac{d_j}{2}\right) - U\left(x - x_j - \frac{d_j}{2}\right)\right] \tag{3.11}$$

Z_{ij} is calculated as

$$Z_{ij} = -\frac{h}{d_j}\left(\int_{x-d_j/2}^{x+d_j/2} E_{zi}\,dx\right)\Bigg|_{\substack{x=x_j \\ y=y_j}} \tag{3.12}$$

$$= -j\omega\mu h \sum_m \sum_n \frac{\psi_{mn}(x_i,y_i)\psi_{mn}(x_j,y_j)}{k^2 - k_{mn}^2} \operatorname{sinc}\left(\frac{md_i}{2a}\right)\operatorname{sinc}\left(\frac{md_j}{2a}\right)$$

Using this expression for the antenna geometry shown in Figure 3.6, the

mutual impedances are obtained as

$$Z_{11} = -j\omega\mu h \sum_m \sum_n \frac{\psi_{mn}^2(x_1, y_1)}{k^2 - k_{mn}^2} \operatorname{sinc}\left(\frac{md_1}{2a}\right) \tag{3.13}$$

$$Z_{22} = -j\omega\mu h \sum_m \sum_n \frac{\psi_{mn}^2(x_2, y_2)}{k^2 - k_{mn}^2} \operatorname{sinc}\left(\frac{md_2}{2a}\right) \tag{3.14}$$

$$Z_{12} = Z_{21} = -j\omega\mu h \sum_m \sum_n \frac{\psi_{mn}(x_1, y_1)\psi_{mn}(x_2, y_2)}{k^2 - k_{mn}^2} \operatorname{sinc}\left(\frac{md_1}{2a}\right) \operatorname{sinc}\left(\frac{md_2}{2a}\right) \tag{3.15}$$

In general, for an N-port antenna, the impedance parameters Z_{ii}'s and Z_{ij}'s are given by the following expressions:

$$Z_{ii} = -j\omega\mu h \sum_m \sum_n \frac{\psi_{mn}^2(x_i, y_i)}{k^2 - k_{mn}^2} \operatorname{sinc}\left(\frac{md_i}{2a}\right) \tag{3.16}$$

$$Z_{ij} = -j\omega\mu h \sum_m \sum_n \frac{\psi_{mn}(x_i, y_i)\psi_{mn}(x_j, y_j)}{k^2 - k_{mn}^2} \operatorname{sinc}\left(\frac{md_i}{2a}\right) \operatorname{sinc}\left(\frac{md_j}{2a}\right) \tag{3.17}$$

In summary, the multi-port analysis of a microstrip antenna with some shorting pins follows the following steps: (i) considers the shorting pins as additional ports; (ii) determines the Z parameters of the resulting N-port network; (iii) implements the boundary conditions at the load terminals, i.e., short circuit terminations are implemented by setting the voltages at the ports to zero; and finally (iv) calculates the input impedance at the feed port. It should be noted that the multi-port analysis is applicable to not only microstrip antennas with shorting pins but also to microstrip antennas with slots in the patch [43]. Although this approach is very useful for the calculation of the input impedance of a microstrip antenna with multiple shorting pins, it can not provide any information on the field distribution under the patch, and hence no

information on the radiation pattern. To remedy this deficiency of the method, a hybrid method, based on the cavity model in conjunction with the method of moments using the point-matching algorithm, is proposed, and detailed in the following chapter.

Chapter 4

Hybrid Model

For a probe-fed microstrip antenna, it is quite common to employ the cavity model to find the field distribution under the patch and other electrical properties. This is mainly because the cavity model provides physical insight on the operation mechanism of microstrip antennas and is computationally efficient as compared to the full-wave analysis of such antennas. However, the cavity model fails in predicting the effect of feeding probe on the field distribution in the cavity completely. Since feeding probe is made of PEC, the electric field under the patch should satisfy the boundary condition on the probe. In the application of the cavity model, this fact is always ignored, with the assumption that the source probe is too thin to affect the field distribution under the patch significantly. The source probe is considered as a current sheet and the only boundary condition applied is the discontinuity in the magnetic field by the amount of the known current source. However, in the development of broadband microstrip antennas, recently wider strips have been used as feeding probes, which significantly alter the resonant frequency and other electrical properties of the antenna.

In addition, as mentioned in the previous chapter, the multi-port analysis is a technique based on the cavity model, and is employed to predict the input impedance of a probe-fed microstrip antenna with shorting strips. In the multi-port analysis, the boundary conditions at the ports of the shorting strips are implemented for the calculation of the input impedance, i.e., setting the voltage at the ports of the shorting strips to zero, the boundary conditions of the tangential electric fields along the shorting conductors are effectively applied. However, this approach does not provide any information about the field distribution under the patch with shorting strips, which is usually used to calculate the radiation properties of the patch antenna.

In this thesis, a hybrid model is developed to remedy the inadequacy of cavity model in accounting for the PEC nature of the feeding probe and the inadequacy of multi-port analysis in predicting the field distribution under the patch with shorting strips. This model is named *hybrid*, because it uses orthogonal modes of the cavity model in finding the **E**-field under the patch and uses the point-matching method in making **E**-field zero on the probe and shorting strips.

This chapter shows how hybrid model calculates the field distribution under the patch with shorting strips and the input impedance at the feed port.

4.1 Derivation of Electric Field under the Patch

The hybrid model considers the feeding probe and shorting strips as current sources with unknown current distributions, contrary to the known current density of the feed in the conventional cavity model. Figure 4.1 shows the top view of a rectangular patch of thickness h with a probe feed and one shorting

strip both lying along x-direction. The feed is located at point (x_p, y_p) and has an effective width d, while the shorting strip is located at point (x_s, y_s) and has an effective width d_s. The unknown current densities on the feed and shorting strip are determined using the point-matching method that implements the boundary condition of the tangential electric field on both conductors. Actually, the implementation of the multi-port analysis via the traditional cavity model is also a point-matching application with only one point.

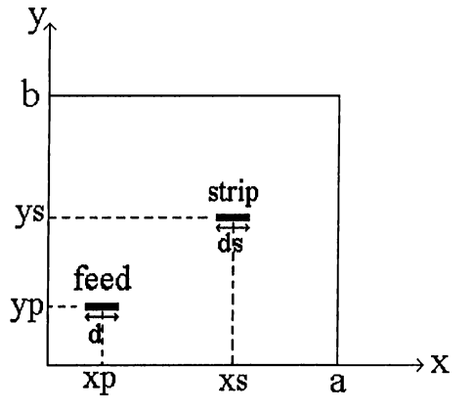

Figure 4.1: Top view of probe-fed rectangular patch with one shorting strip.

The point-matching method is a special form of the method of moments (MoM), which is most commonly used technique to solve for an unknown function in an operator equation. In electromagnetic applications, these operators are usually differential, integral or integro-differential operators, and these are converted to matrix equations with the help of the MoM. The procedure of the MoM to transform an operator equation to a matrix equation starts with writing the unknown function in terms of known basis functions with unknown coefficients, by which the operator equation is transformed to an algebraic equation. Then, implementing boundary conditions at as many points as the number of unknowns generates the matrix equation with the

unknown coefficients as the vector to be determined. If the implementation of the boundary conditions is performed at discrete points, rather than weighting the algebraic equation with some functions and implementing the boundary conditions in integral sense, the procedure is named as point matching. For the problem at hand, the current density along the vertical conductors is written in terms of pulse basis functions, Fig.4.2, as

$$\mathbf{J}_{\text{feed}} = \hat{\mathbf{z}} \sum_{l=1}^{N} I_l \tilde{\delta}(y - y_p) \left[U\left(x - x_l + \frac{d}{2N} \right) - U\left(x - x_l - \frac{d}{2N} \right) \right] \frac{N}{d} \tag{4.1}$$

for the feed, and

$$\mathbf{J}_{\text{strip}} = \hat{\mathbf{z}} \sum_{l=1}^{M} I_{sl} \tilde{\delta}(y - y_s) \left[U\left(x - x_{sl} + \frac{d_s}{2M} \right) - U\left(x - x_{sl} - \frac{d_s}{2M} \right) \right] \frac{M}{d_s} \tag{4.2}$$

for the shorting strip,

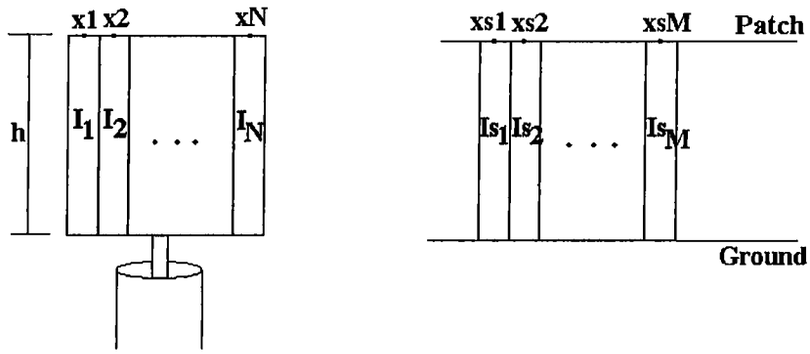

(a) (b)

Figure 4.2: Point matching application (a) on the probe feed with N points, (b) on the shorting strip with M points

where I_l's and I_{sl}'s are unknown amplitudes. Note that N/d in $\mathbf{J}_{\text{feed}}$ and M/d_s in $\mathbf{J}_{\text{strip}}$ is used to make the total current on the feed and on the shorting strip equal to $I_1+...+I_N$ and $I_{s1}+...+I_{sM}$, respectively. With these current densities, the total **E**-field under the patch is written as a linear superposition of the contributions of both current densities,

$$\mathbf{E}_{\text{z-total}}(x,y)=\mathbf{E}_{\text{z-feed}}(x,y)+\mathbf{E}_{\text{z-strip}}(x,y) \tag{4.3}$$

where $\mathbf{E}_{\text{z-feed}}$ and $\mathbf{E}_{\text{z-strip}}$ are the electric fields generated by the feed current and the shorting-strip current, respectively.

In the cavity model, as presented in Chapter 2, Green's function G_z, due to an impulse source at point (x',y'), is determined as:

$$G_z(x,y;x',y')=\sum_m\sum_n \frac{\psi_{mn}(x',y')\psi_{mn}(x,y)}{k^2-k_{mn}^2} \tag{4.4}$$

Then, because of the linearity of the system, $\mathbf{E}_{\text{z-feed}}$ is written as the convolution integral of G_z and $\mathbf{J}_{\text{feed}}$, while for $\mathbf{E}_{\text{z-strip}}$, G_z and $\mathbf{J}_{\text{strip}}$ are convolved, resulting in:

$$E_{z\_feed}(x,y)=j\omega\mu\sum_{l=1}^{N} I_l\left(\sum_m\sum_n \frac{\psi_{mn}(x_l,y_p)\psi_{mn}(x,y)}{k^2-k_{mn}^2}\operatorname{sinc}\left(\frac{md}{2aN}\right)\right) \tag{4.5}$$

$$E_{z\_strip}(x,y)=j\omega\mu\sum_{l=1}^{M} I_{sl}\left(\sum_m\sum_n \frac{\psi_{mn}(x_{sl},y_s)\psi_{mn}(x,y)}{k^2-k_{mn}^2}\operatorname{sinc}\left(\frac{md_s}{2aM}\right)\right) \tag{4.6}$$

Once these algebraic equations are obtained for the electric fields in terms of the unknown coefficients of the pulse basis functions, these unknown coefficients, I_l's and I_{sl}'s, can be obtained by imposing the boundary condition onto the total electric field on the sections of the feeding strip and shorting strip:

$$E_{z-total}(x_l,y_p)=0 \qquad for\ l = 1,2,...,N \tag{4.7}$$

$$E_{z-total}(x_{sl},y_p)=0 \qquad for\ l = 1,2,...,M \tag{4.8}$$

This results in a homogeneous matrix equation

$$AI=0 \tag{4.9}$$

where the matrix **A** has the following entries:

$$A_{ij} = \begin{cases} \sum_m \sum_n \dfrac{\psi_{mn}(x_i, y_p)\psi_{mn}(x_j, y_p)}{k^2 - k_{mn}^2} \operatorname{sinc}\left(\dfrac{md}{2aN}\right) & \mathbf{i \le N, j \le N} \\ \sum_m \sum_n \dfrac{\psi_{mn}(x_{si}, y_s)\psi_{mn}(x_{j-N}, y_p)}{k^2 - k_{mn}^2} \operatorname{sinc}\left(\dfrac{md_s}{2aM}\right) & \mathbf{i \le N, N \le j \le N+M} \\ \sum_m \sum_n \dfrac{\psi_{mn}(x_{i-N}, y_p)\psi_{mn}(x_{sj}, y_s)}{k^2 - k_{mn}^2} \operatorname{sinc}\left(\dfrac{md}{2aN}\right) & \mathbf{N \le i \le N+M, j \le N} \\ \sum_m \sum_n \dfrac{\psi_{mn}(x_{si-N}, y_s)\psi_{mn}(x_{sj-N}, y_s)}{k^2 - k_{mn}^2} \operatorname{sinc}\left(\dfrac{md_s}{2aM}\right) & \mathbf{N \le i \le N+M,\ N \le j \le N+M} \end{cases}$$

and (4.10)

$$I = [I_1 \quad \cdots \quad I_N \quad I_{s1} \quad \cdots \quad I_{sM}]^T \tag{4.11}$$

For the nontrivial solution of (4.9), the matrix A should be singular, i.e., *det(A) = 0*. The frequencies for which this condition is satisfied are known as the *natural resonant frequencies* of the patch, which are the eigenvalues of the cavity. Since these frequencies are eigenvalues of the cavity, with corresponding eigenmodes, that do not include the effects of other modes, they are not the actual operation frequencies of the antenna. The lowest resonant frequency is used to find the current distribution $I_1,...,I_N$ on the feed, as described in the following paragraph.

The condition that the current on the feed is 1 Amp, that is $I_1+...+I_N = 1$, adds one more row to the matrix **A**. The resulting matrix equation, then, becomes

$$\left[\begin{array}{c|c} A^{f,f}_{n,n} & A^{s,f}_{n,m} \\ N\times N & N\times M \\ \hline A^{f,s}_{m,n} & A^{s,s}_{m,m} \\ M\times N & M\times M \\ \hline 1 & 0 \\ 1\times N & 1\times M \end{array}\right]\left[\begin{array}{c} I_n \\ N\times 1 \\ \hline I_{sm} \\ M\times 1 \end{array}\right]=\left[\begin{array}{c} 0 \\ (M+N)\times 1 \\ \hline 1 \end{array}\right] \tag{4.12}$$

where *f,f* refers to the field component created by the feed and evaluated at the feed position; *s,f* refers to the field component created by the strip and evaluated at the feed position; *f,s* refers to the field component created by the feed and evaluated at the strip position; *s,s* refers to the field component created by the strip and evaluated at the strip position.

Since the matrix equation, Eq.(4.12), is over-determined, $N+M$ unknowns but $N+M+1$ equations, its solution is not unique. Therefore, the least square solution is obtained at the resonant frequency of the cavity, which gives the current distribution both on the feed probe and on the shorting strip. The current distribution $I_1,...I_N$ found for the feed is accepted as the final distribution, and independent of the excitation frequency, if it is in the near vicinity of the resonant frequency of the cavity. However, the current distribution at the shorting strip, $I_{s1},...I_{sM}$, is determined at each frequency by solving

$$A'I'=b \tag{4.13}$$

where

$$A_{ij}'=\sum_m\sum_n \frac{\psi_{mn}(x_{si},y_s)\psi_{mn}(x_{sj},y_s)}{k^2-k_{mn}^2}\operatorname{sinc}\left(\frac{md_s}{2aM}\right) \tag{4.14}$$

$$I'=[I_{s1}\quad\cdots\quad I_{sM}]^T \tag{4.15}$$

$$b_i = -E_{z-feed}(x_{si}, y_s) \tag{4.16}$$

In this model, as a summary, the feed current is kept constant at its value determined at the resonant frequency of the cavity, but the current on the shorting strip is calculated at each excitation frequency using (4.13). Once the current distributions are determined, the total **E** field under the patch can be calculated at each frequency.

The feeding probe and shorting pin (modelled as strips) used in this derivation are both extended along x-direction. For y-extended feed and shorting strips, the same derivation is used, except that sectioning is performed in y direction. The resulting current distributions and electric fields are:

$$\mathbf{J}_{\text{feed}} = \hat{\mathbf{z}} \sum_{l=1}^{N} I_l \tilde{\delta}(x - x_p) \left[U\left(y - y_l + \frac{d}{2N} \right) - U\left(y - y_l - \frac{d}{2N} \right) \right] \frac{N}{d} \tag{4.17}$$

$$\mathbf{J}_{\text{strip}} = \hat{\mathbf{z}} \sum_{l=1}^{M} I_{sl} \tilde{\delta}(x - x_s) \left[U\left(y - y_{sl} + \frac{d_s}{2M} \right) - U\left(y - y_{sl} - \frac{d_s}{2M} \right) \right] \frac{M}{d_s} \tag{4.18}$$

$$E_{z\_feed}(x, y) = j\omega\mu \sum_{l=1}^{N} I_l \left(\sum_m \sum_n \frac{\psi_{mn}(x_p, y_l)\psi_{mn}(x, y)}{k^2 - k_{mn}^2} \operatorname{sinc}\left(\frac{nd}{2bN} \right) \right) \tag{4.19}$$

$$E_{z-strip}(x, y) = j\omega\mu \sum_{l=1}^{M} I_{sl} \left(\sum_m \sum_n \frac{\psi_{mn}(x_s, y_{sl})\psi_{mn}(x, y)}{k^2 - k_{mn}^2} \operatorname{sinc}\left(\frac{nd_s}{2bM} \right) \right) \tag{4.20}$$

Note that this approach can easily be used for patches without shorting strips, where the current distribution on the feed found at the resonant frequency of the cavity (the frequency where the determinant is zero) is used at all frequencies.

Once the electric field under the patch is determined, H field can be determined using Maxwell's equations. Then, far zone fields and quality factor

can be calculated using the same steps given in Chapter 2.

4.2 Input Impedance Calculation

Since the hybrid model enforces the tangential electric field to be zero on the feeding conductor, the formulas given in Chapter 2 for the input impedance can not be used in this model. So, the input impedance is calculated by

$$Z_{in} = \frac{P_l + 2j\omega(W_e - W_M)}{\frac{1}{2}|I|^2} \tag{4.21}$$

where

$P_l = P_d + P_c + P_r$: Power loss

W_e: stored electric energy

W_m: stored magnetic energy

I: Total current on the probe (1 Amp),

and the formulas for P_l, W_e and W_m are the same as those given in Chapter 2.

Chapter 5

Simulations and Experimental Results

The hybrid model, explained in detail in Chapter 4, presents an analysis technique for microstrip antennas, which accounts for vertical conductors such as wide feeding strips and shorting strips. Its difference from the conventional cavity model and the multi-port analysis is that it provides accurate field distribution under the patch with vertical conductors. To verify the accuracy of the hybrid model, the following two properties of the patches are examined in the simulations:

- The zero tangential electric field condition on the conductors,
- The resonant frequency of the patch, which is actually calculated from the electric field under the patch.

The resonant frequency is determined as the frequency at which the input impedance matches to 50Ω, namely the frequency at which the input reflection

coefficient

$$\Gamma_{in} = \frac{Z_{in} - 50}{Z_{in} + 50} \tag{5.1}$$

has minimum magnitude. The resonant-frequency results of the hybrid model are then compared to those obtained from the multi-port analysis and from experimental measurements. The verification of the hybrid model is first performed for the patch antennas with wide vertical feeds, and then for the patch antennas with shorting strips.

In the simulations, the effective patch dimensions, due to the fringing fields, are calculated using the edge-extension formulas given in Appendix A. The effective width of the feed and strips are chosen the same as their physical widths. The double summations in the formulas derived in Cavity Model and multi-port analysis are reduced to single summations, which are given in Appendix B. In the simulations of hybrid model, a dynamic convergence criterion is used. For the dynamic convergence, the limits of the summations are increased until the differences between two subsequent summations are less than an error criterion, which is chosen as 10^{-7} in this study.

For the experimental study, due to the difficulty in soldering, air is chosen between the patch and the ground plane instead of a dielectric substrate, and the thickness is chosen thicker than the usual antennas. The conductors used for both the patch and ground plane are made of bronze with a conductivity of 10^5 mho/cm. The side view of the antennas used in this study is shown in Figure 5.1, for which the top view of the patch in Figure 4.1 is taken as the basis. For the sake of coherence of the thesis, Figure 4.1 is repeated here again as Figure 5.2.

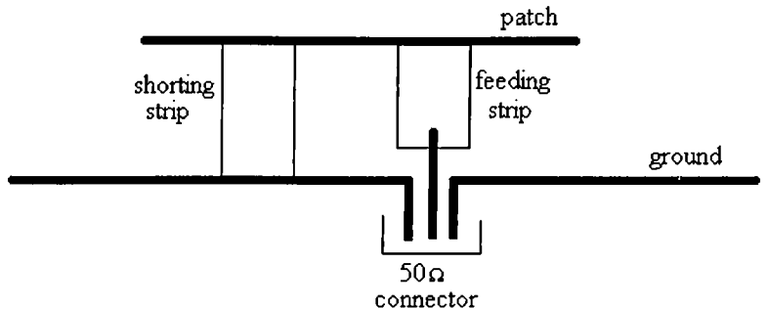

Figure 5.1: Side view of antennas used in the experiments.

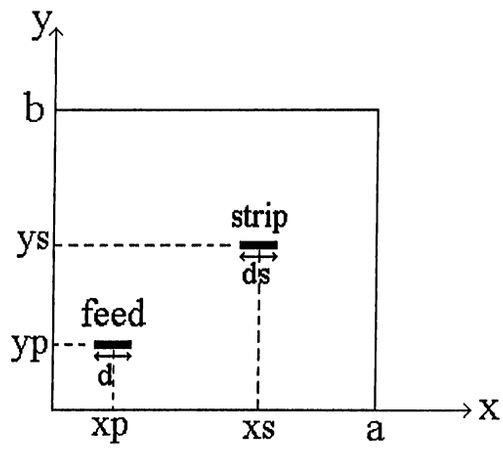

Figure 5.2: Top view of a probe-fed patch with a shorting strip

5.1 Results for Patches with Wide Vertical Feeds

The hybrid model is first applied to microstrip antennas with wide vertical feeds extended in x-direction. For these antennas, the lowest resonant frequencies, which are the resonant frequencies of (0,1) modes, are evaluated by the use of the available techniques, the cavity model and the hybrid model, and compared to the results obtained from experimental measurements. In addition, to observe the effect of the hybrid model on the electric field

distribution along the feed in the cavity, the normalized magnitudes of the electric fields are provided under the patch.

The geometrical parameters of the first antenna constructed in this study are reported in Table 5.1, and the resonant frequencies calculated and measured for this antenna are given in Table 5.2. The normalized magnitude of the electric field under the patch along the x direction, at the plane of the feed $y = y_p$, is shown in Figure 5.3, as obtained from both the cavity model and hybrid model. In addition, to demonstrate the close match between the input impedance patterns obtained theoretically and experimentally, the measured and calculated input impedance locii are given in Figure 5.4 for this specific antenna. The number of sections on the feed in the hybrid model is chosen 9. The geometrical parameters of the second antenna, with the same number of sections on the feed as the first antenna, its resonant frequencies and the normalized magnitude of the electric field are given in Tables 5.3, 5.4 and Figure 5.5, respectively. The last antenna has the same properties as the second one except that the width of the feed conductor is 1.5 cm, and that the number of sections used on the feed is chosen as 11. The resonant frequencies and the normalized magnitudes of the electric fields corresponding to this antenna are given in Table 5.5 and Figure 5.6, respectively.

From these results, it is observed that the resonant frequencies obtained from the hybrid model are in good agreement with those obtained from the cavity model and experimental results. In addition, the input impedances obtained by the hybrid model agree with the experimental results quite well, much better than the results predicted by the conventional cavity model, as shown in Fig. 5.4. The best of all, the boundary condition of the tangential

electric fields at the feeding strips is observed now to be satisfied, see Figs. 5.3, 5.5 and 5.6. Note that, the tangential electric fields at the feeding strips obtained from the cavity model become maximum, because, as mentioned earlier in this thesis, the traditional cavity model assumes these feeding strips as current sheets. Although the differences of the field distributions at the feed plane, obtained from the hybrid method and cavity model, are quite significant for all three antennas, the resonant frequencies calculated by the same methods are very close. This could be attributed to the fact that the feed structures are always small as compared to the patches, and hence changes in the field distribution just in the near vicinity of the feed do not affect the global parameters like the resonant frequency.

a(cm)	b(cm)	h(cm)	ε_r	x_p(cm)	y_p(cm)	d(cm)
8.0	10.0	0.6	1	4.0	3.0	1.0

Table 5.1: Properties of the first antenna

Case	f_r (GHz)	$\|\Gamma in\|$
Cavity Model	1.37	0.335
Zero Determinant	1.51	-
Hybrid Model	1.35	0.367
Experiment	1.34	0.414

Table 5.2: Calculated and measured resonant frequencies for the antenna with properties given in Table 5.1

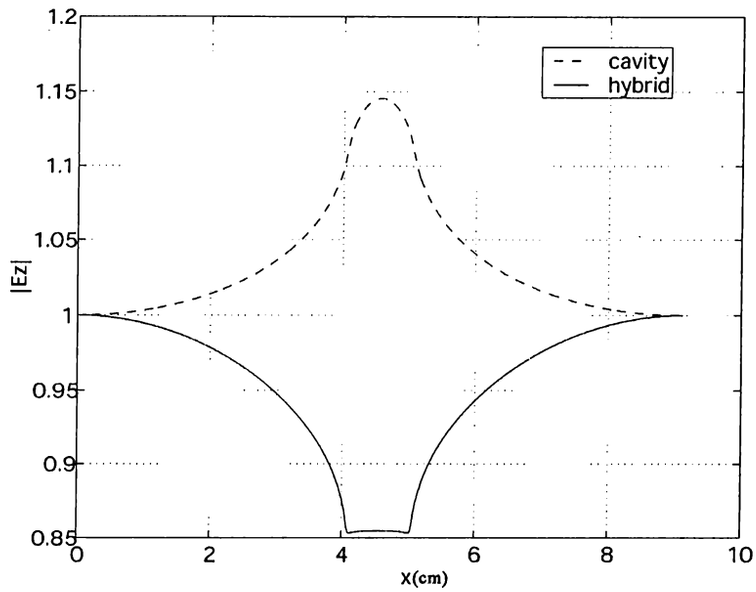

Figure 5.3: Normalized $|E_z|$ under the first patch at $y = y_p$.

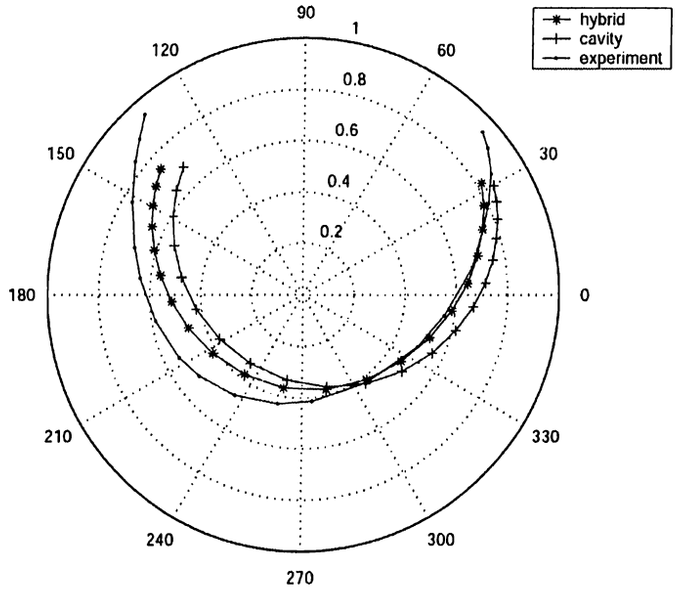

Figure 5.4: Measured and calculated input impedance locii for the first antenna

a(cm)	b(cm)	h(cm)	ε_r	x_p(cm)	y_p(cm)	d(cm)
5.0	6.0	0.6	1	2.5	2.0	1.0

Table 5.3: Properties of the second antenna

Case	f_r (GHz)	$\|\Gamma in\|$
Cavity Model	2.18	0.046
Zero Determinant	2.35	-
Hybrid Model	2.18	0.048
Experiment	2.16	0.037

Table 5.4: Calculated and measured resonant frequencies for the antenna with properties given in Table 5.3

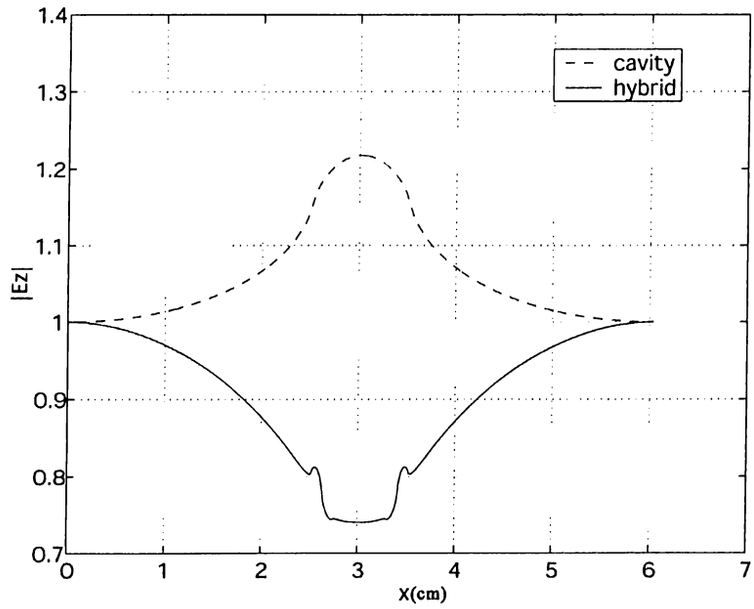

Figure 5.5: Normalized $|E_z|$ under the second patch at $y = y_p$.

Case	f_r (GHz)	$\|\Gamma in\|$
Cavity Model	2.17	0.096
Zero Determinant	2.40	-
Hybrid Model	2.16	0.061
Experiment	2.14	0.042

Table 5.5: Calculated and measured resonant frequencies for the third antenna

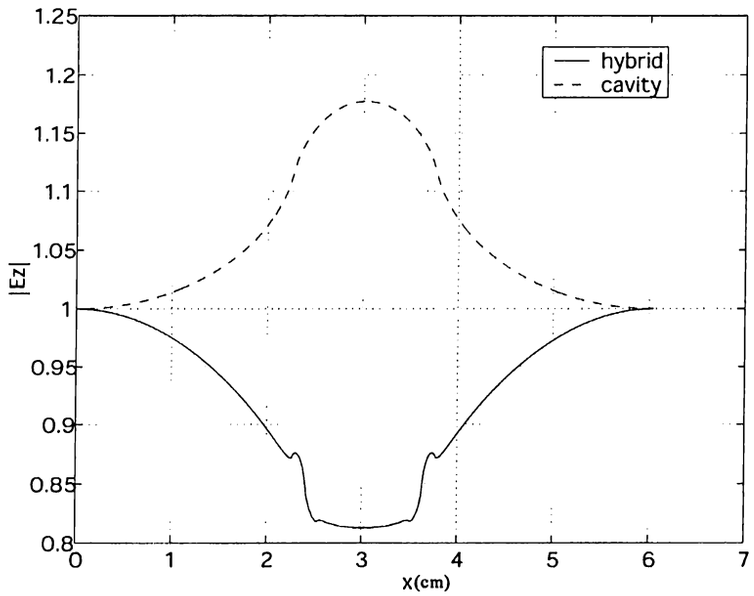

Figure 5.6: Normalized $|E_z|$ under the third patch at $y = y_p$.

5.2 Results for Patches with Shorting Strips

After having introduced the hybrid method and observed its contributions, as compared to the traditional cavity model, on the electrical characteristics of the microstrip antennas with probe feed, it is now applied to microstrip antennas with wide vertical feeds and shorting strips. As it was mentioned earlier, for the dual-band operation, shorting strips are usually placed on the nodal line of E_z corresponding to the mode whose resonant frequency is kept constant, (0,3) mode

in this study, while the resonant frequency of the other mode, (0,1) mode, is varied via the shorting strips. In the antennas designed with shorting strips, the dual frequency operation is tested, where the resonant frequencies of (0,1) mode and (0,3) mode are evaluated. The resonant frequencies calculated using both multi-port analysis and hybrid model are compared with the ones obtained from the measurements. In addition, electric field distribution under the patch, specifically at the planes of the feed and the shorting strips, is calculated to observe how the boundary condition at the feeding and shorting strips are satisfied. Due to the experimental difficulties in constructing the antennas, only one shorting strip is used in these antennas.

The first antenna designed, with probe and shorting strips extending in x-direction laterally, has the properties reported in Table 5.6. Calculated and measured resonant frequencies corresponding to (0,1) mode, f_l, and (0,3) mode, f_h, are given in Table 5.7. Since the network analyzer used in the experiments was not able to measure frequencies higher than 6 GHz, the f_h could not be measured for this antenna, and hence no experimental result for this frequency in Table 5.7. Normalized magnitudes of the electric field under the patch, corresponding to the lower mode, are obtained from the hybrid model, and are shown in Figures 5.7 and 5.8. They represent the electric field $|E_z|$ at the positions of the feed and shorting strip, respectively, along the lateral dimensions of these strips, x-direction for this problem. Similarly, normalized magnitudes of the electric field under the patch corresponding to the higher mode are shown in Figures 5.9 and 5.10, where they represent the electric field $|E_z|$ at the positions of the feed and shorting strip, respectively. In the hybrid model, the number of sections on the feed and shorting strip are chosen 5 and

9, respectively.

The properties of the second antenna, namely its resonant frequencies for both modes, and normalized magnitudes of the electric field at the feed position and shorting-strip position for both the low and high modes are given in Tables 5.8, 5.9, and Figures 5.11 - 5.14, respectively. To demonstrate the agreement between the calculated and measured input impedance patterns, this specific antenna is selected among the patches with shorting strips. So, the calculated and measured input impedance locii for the low mode are given in Figure 5.15, and for the high mode in Figures 5.16, 5.17. Note that both feed and shorting strips are extended in x-direction laterally, and the number of sections on the strips are 5 and 9, respectively.

The last antenna has the same properties as the second one except that the width of the shorting strip is 1.0 cm and extended in y-direction laterally. The resonant frequencies and normalized electric field magnitudes at the positions of the feed and shorting strips, for the low mode and high mode corresponding to this antenna, are given in Table 5.10, and Figures 5.18 - 5.21, respectively. The number of sections on the feed and shorting strips are chosen as 5 and 9 for this antenna.

a	b	h	ε_r	x_p	y_p	x_s	y_s	d	d_s
5.0	6.0	0.65	1	2.4	0.0	2.5	1.0	0.45	1.0

Table 5.6: Properties of the first antenna with a shorting strip. Dimensions are in cm.

Case	f_l (GHz)	$\|\Gamma in_l\|$	f_h(GHz)	$\|\Gamma in_h\|$	f_h/f_l
Cavity Model for No strip Case	2.44	0.462	6.08	0.371	2.49
Multi-port	2.80	0.057	6.13	0.172	2.19
Zero Determinant	2.87	-	6.20	-	2.16
Hybrid Model	2.84	0.113	6.14	0.161	2.16
Experiment	2.74	0.132	-	-	-

Table 5.7: Resonant frequencies and the corresponding reflection coefficients of the antenna with properties given in Table 5.6.

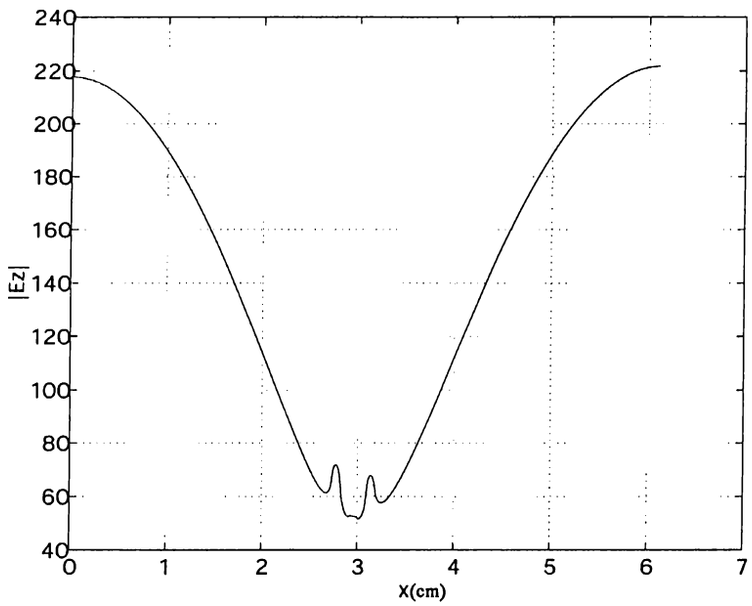

Figure 5.7: Normalized $|E_z|$ of the low mode under the first patch at the feed position $y = y_p$, obtained by the hybrid model. Dimensions are effective.

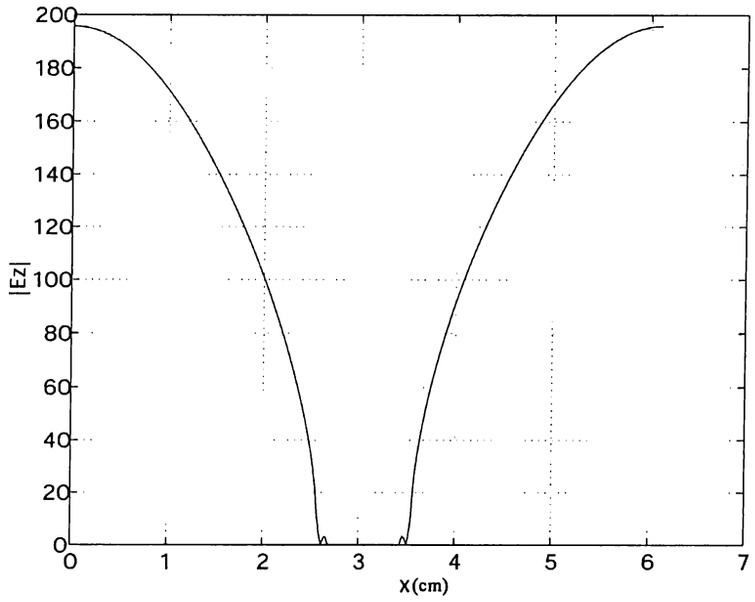

Figure 5.8: Normalized $|E_z|$ of the low mode under the first patch at the position of the shorting strip $y = y_s$, obtained by the hybrid model. Dimensions are effective.

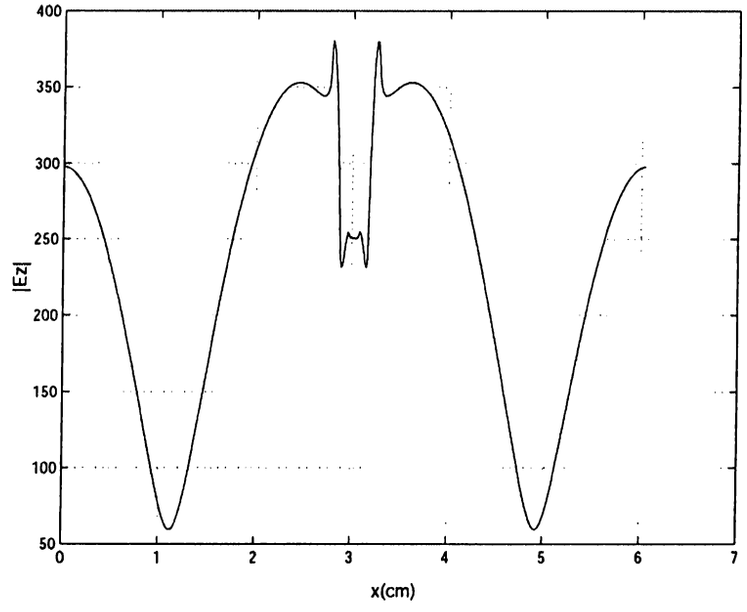

Figure 5.9: Normalized $|E_z|$ of the high mode under the first patch at the feed position $y = y_p$, obtained by the hybrid model. Dimensions are effective.

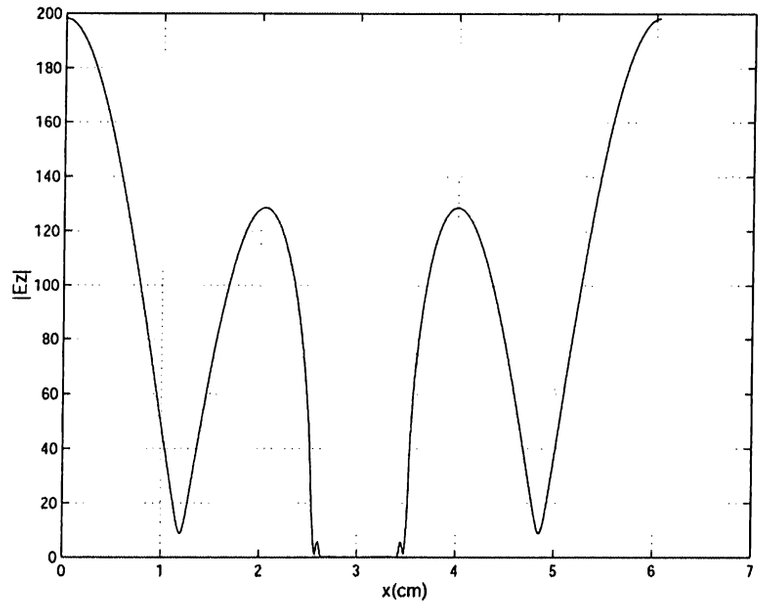

Figure 5.10: Normalized $|E_z|$ of the high mode under the first patch at the position of the shorting strip $y = y_s$, obtained by the hybrid model. Dimensions are effective.

a	b	h	ε_r	x_p	y_p	x_s	y_s	d	d_s
8.0	10.0	0.6	1	4.0	0.0	4.0	1.7	0.5	1.5

Table 5.8: Properties of the second antenna with a shorting strip. Dimensions are in cm.

Case	f_l (GHz)	$\|\Gamma in_l\|$	f_h(GHz)	$\|\Gamma in_h\|$	f_h/f_l
Cavity Model for No Strip Case	1.48	0.620	3.95	0.283	2.67
Multi-port	1.79	0.227	4.09	0.434	2.29
Zero Determinant	1.85	-	4.75	-	2.57
Hybrid Model	1.75	0.065	4.12	0.406	2.35
Experiment	1.71	0.067	4.07	0.423	2.38

Table 5.9: Resonant frequencies and the corresponding reflection coefficients of the antenna with properties given in Table 5.8.

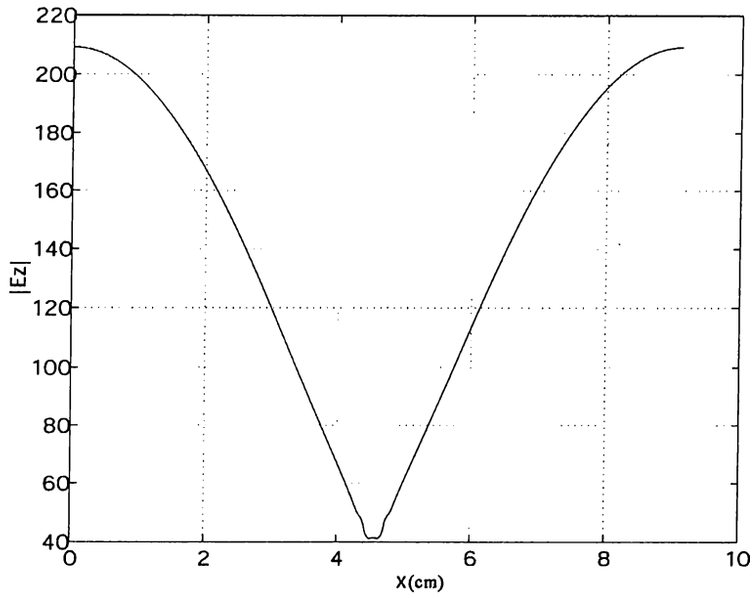

Figure 5.11: Normalized $|E_z|$ of the low mode under the second patch at the feed position $y = y_p$, obtained by the hybrid model. Dimensions are effective.

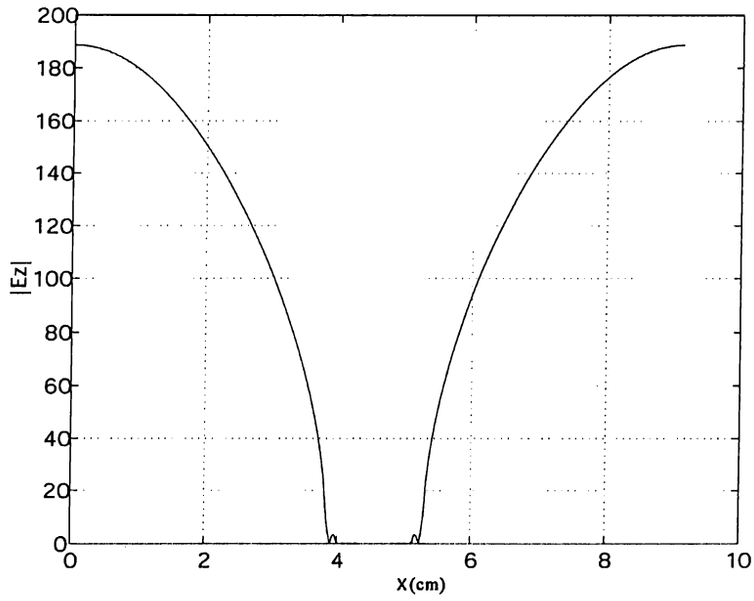

Figure 5.12: Normalized $|E_z|$ of the low mode under the second patch at the position of the shorting strip $y = y_s$, obtained by the hybrid model. Dimensions are effective.

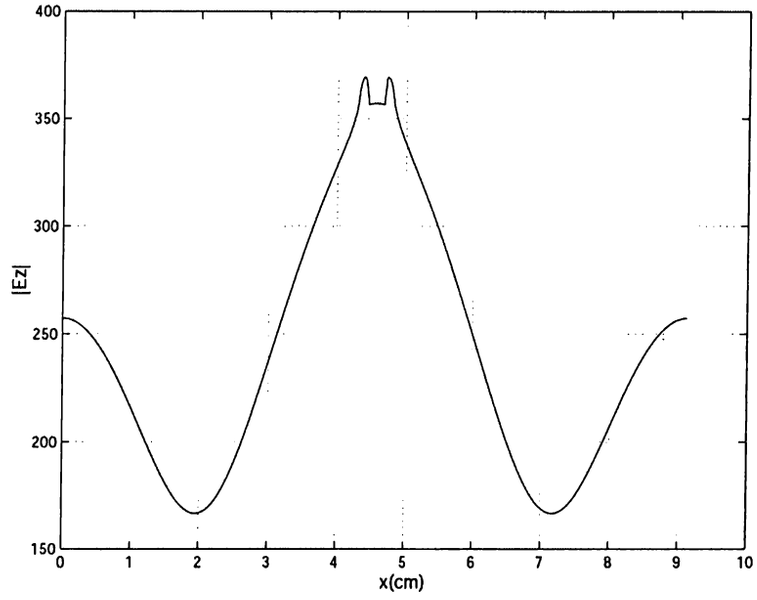

Figure 5.13: Normalized $|E_z|$ of the high mode under the second patch at the feed position $y = y_p$, obtained by the hybrid model. Dimensions are effective.

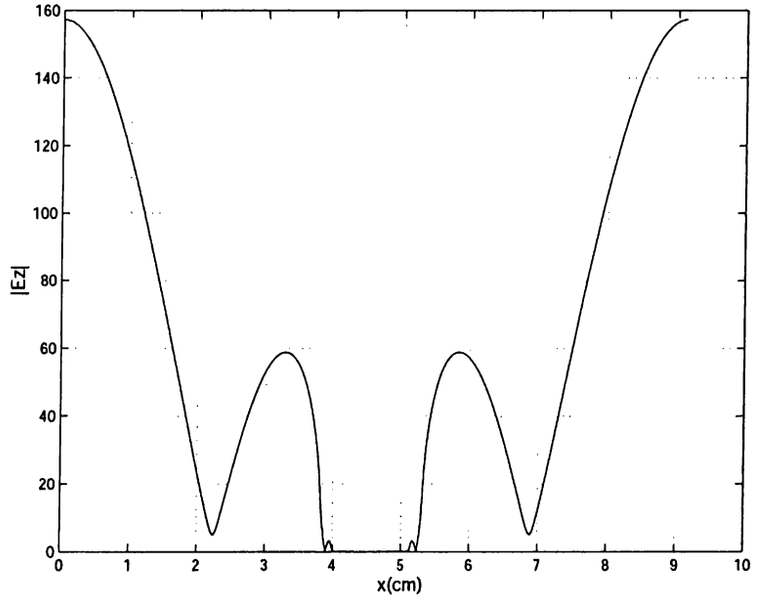

Figure 5.14: Normalized $|E_z|$ of the high mode under the second patch at the position of the shorting strip $y = y_s$, obtained by the hybrid model. Dimensions are effective.

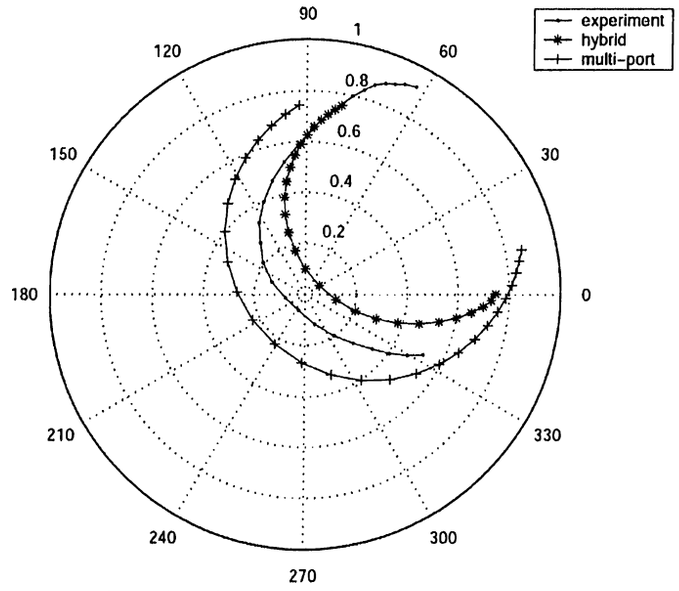

Figure 5.15: Measured and calculated low mode input impedance locii for the second antenna.

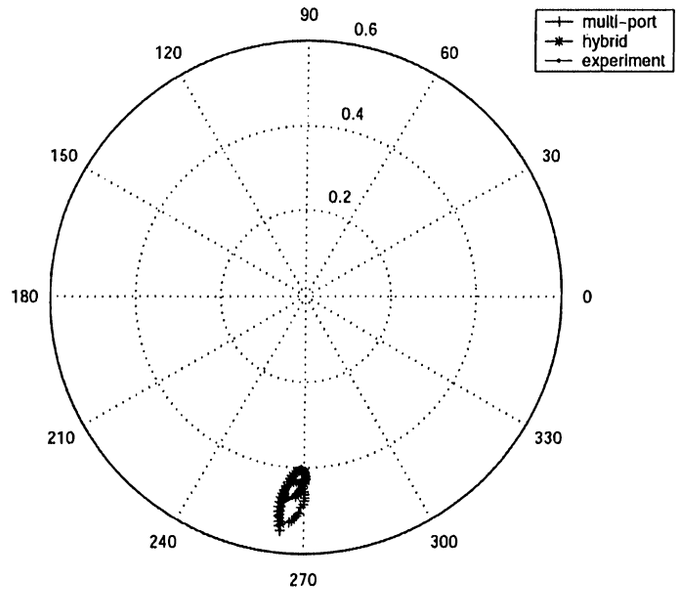

Figure 5.16: Measured and calculated high mode input impedance locii for the second antenna (normal view).

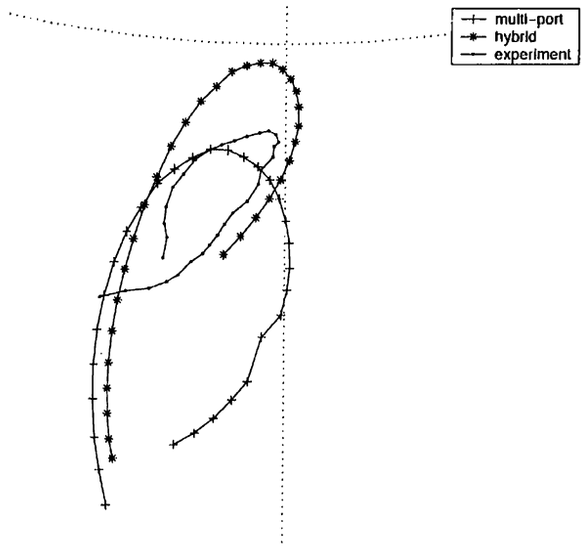

Figure 5.17: Measured and calculated high mode input impedance locii for the second antenna (zoomed view).

Case	f_l (GHz)	$\|\Gamma in_l\|$	f_h(GHz)	$\|\Gamma in_h\|$	f_h/f_l
Cavity Model for No Strip Case	1.48	0.620	3.95	0.283	2.67
Multi-port	1.72	0.311	4.05	0.496	2.35
Zero Determinant	1.79	-	4.79	-	2.68
Hybrid Model	1.73	0.198	4.09	0.517	2.36
Experiment	1.70	0.112	4.07	0.392	2.39

Table 5.10: Resonant frequencies and the corresponding reflection coefficients of the third antenna with a shorting strip.

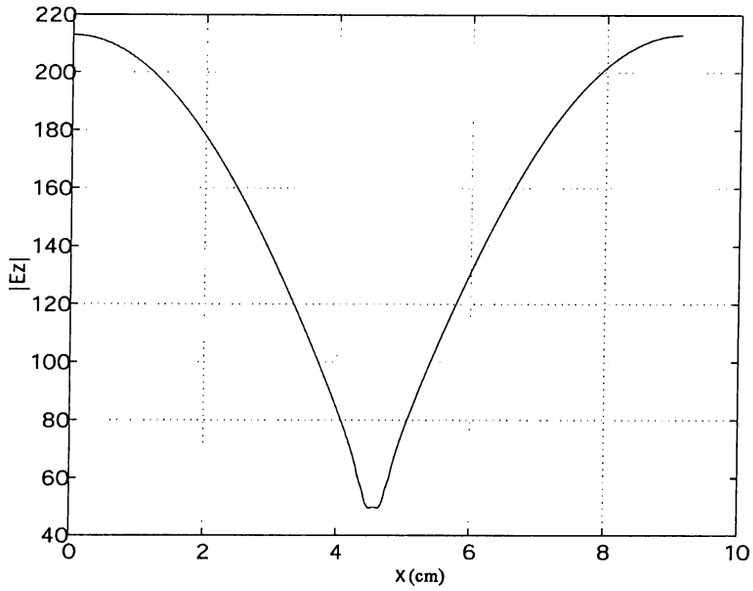

Figure 5.18: Normalized $|E_z|$ of the low mode under the third patch at the feed position $y = y_p$, obtained by the hybrid model. Dimensions are effective.

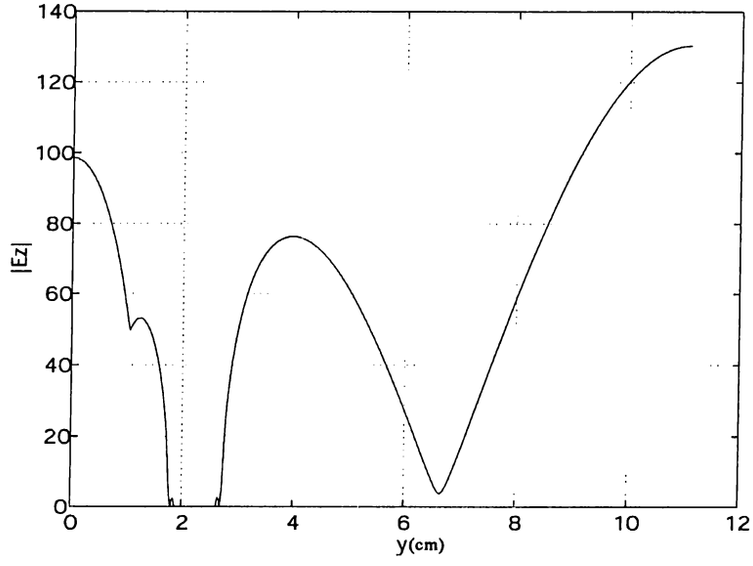

Figure 5.19: Normalized $|E_z|$ of the low mode under the third patch at the position of the shorting strip $x = x_s$, obtained by the hybrid model. Dimensions are effective.

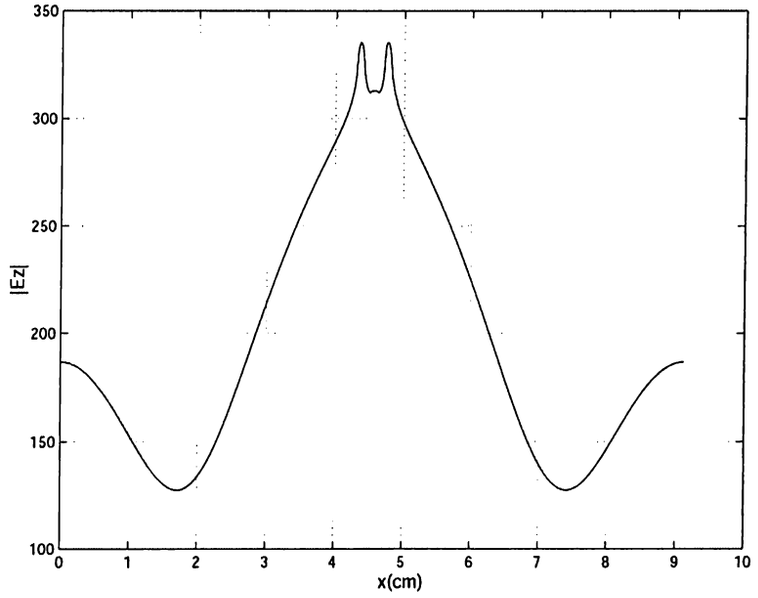

Figure 5.20: Normalized $|E_z|$ of the high mode under the third patch at the feed position $y = y_p$, obtained by the hybrid model. Dimensions are effective.

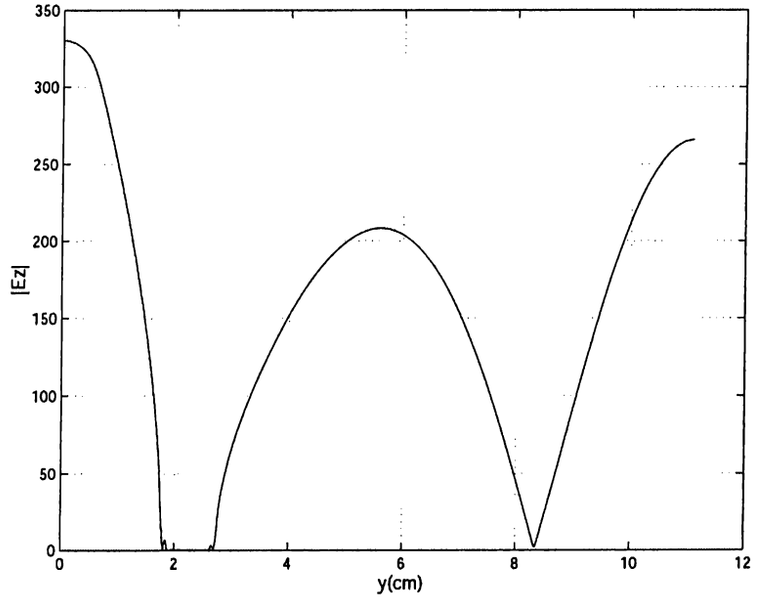

Figure 5.21: Normalized $|E_z|$ of the low mode under the third patch at the position of the shorting strip $x = x_s$, obtained by the hybrid model. Dimensions are effective.

Resonant frequencies obtained from the hybrid model are in good agreement with the experimental results and the multi-port results. It is observed that the multi-port analysis generally predicts the resonant frequencies closer to the experimental results than the hybrid model predicts. However, the hybrid model is more successful in determining the reflection coefficient, and hence the input impedance pattern. It is further observed that, the hybrid model satisfies the boundary condition of the tangential electric field on the vertical conductors. It successfully implements the zero tangential electric field on the shorting strips, while it minimizes the tangential electric field, E_z, on the feeding strip. The reason for not being able to satisfy the boundary condition at the feed can be attributed to the fact that the boundary condition at the feed is applied only at the resonant frequency of the cavity (denoted as zero-determinant in Tables 5.7, 5.9 and 5.10), not at the resonant frequency of the antenna and at the other frequencies of interest. With this implementation, the excitation current distribution is obtained and kept constant at the other frequencies, and hence, a slight deviation at the tangential electric field on the feeding strip is observed at the other frequencies.

Since the main motivation of this study is to assess the amount of frequency shift due to shorting strips for dual-band operation, the results provided in this chapter demonstrate the effect of shorting strips in minimizing f_h/f_l ratio, when placed on the nodal lines of (0,3) mode. Note that, due to the experimental constraints, shorting strips are placed on the nodal line that is closest to the feed side. In the first antenna, the ratio of f_h/f_l without shorting strips was found 2.49, whereas insertion of a shorting strip reduced this ratio to 2.16, as predicted by the hybrid model. The same type of reduction in the ratio of f_h/f_l is observed for the

other antennas, namely, for the second antenna, this ratio reduces from 2.67 to 2.35, and for the last antenna from 2.67 to 2.36 with the insertion of shorting strips. These observations, which are based on the hybrid method, are also verified by the experimental study and the results by the multi-port analysis.

Chapter 6

Optimization Using Genetic Algorithm (GA)

Genetic algorithm is a search algorithm based on the principles of natural genetics. Within the concept of microstrip antennas, genetic algorithm has been used in the design of some antennas with some given specifications [60-64]. This chapter first gives the theory behind GA and then represents some design results of microstrip antennas with shorting strips for the dual frequency operation optimizing the location and width of the shorting strips.

6.1 Theory of Genetic Algorithm

In the literature, there are three main types of search methods:

- Calculus-based
- Enumerative

- Random

Calculus-based methods have two subgroups: indirect methods and direct methods. Indirect methods search the local optima by solving the nonlinear set of equations that result from setting the gradient of the objective function equal to zero. Direct methods search the local optima by hopping on the function and moving in a direction related to the local gradient. These methods suffer from two disadvantages: First, they have local scope of search, namely the optimum point they find depends on the starting point. If the search starts in the neighborhood of a local optimum point, the method converges to that point and misses the main event. Second, these methods are based on the derivatives. The nonexistence of derivatives in many objective functions limits the use of this method.

Enumerative methods look at the values of the objective functions at every point in a finite search space and find the optima. Since the search spaces are too large to search one at a time for most of the practical problems, this method is inefficient and time consuming.

The main idea behind random methods is to search semi-randomly and to save the best. Two popular examples in this category are genetic algorithms and simulated annealing. Note that, although random search methods are random, they are not completely directionless.

Genetic algorithms use random choice as a tool to search through a coding of a parameter space. It is developed by John Holland and his colleagues in the early 1970's. Their main aim in doing research on genetic algorithms was to provide robustness in artificial systems that perform high levels of efficiency. GA differs from other optimization methods in the following ways:

- It works with a coding of the parameter set, not the parameters themselves.
- It searches from a population of points, not a single point.
- It uses the objective function directly, not its derivatives or other knowledge dependent on the objective function.
- It uses probabilistic rules, not deterministic rules.

GA mimics the features of natural genetics in finding the optima, which has the following main features:

- Evaluation takes place on chromosomes that are organic devices for encoding the structure of living beings.
- Natural selection causes the chromosomes that encode successful structures to reproduce more often than those that do not.
- Recombination processes combine material from chromosomes of two parents and create quite different chromosomes in the children.
- Mutations cause the chromosomes of children differ from those of their parents.

In genetic algorithm, the first step is to code the parameter set of the optimization as a finite-length string that is also called a *chromosome*. A simple coding can be generated by considering a chromosome of 1's and 0's. GA generates a population of these chromosomes rather than a single chromosome, and then generates successive populations of chromosomes. Therefore, GA increases the probability of finding the right optimum point by searching the whole parameter space in a parallel manner. The initial population is chosen at random by simply using coin flips. The next step is to evaluate this population of chromosomes. GA has no need for any extra information such as derivative to

perform the search except for the objective function values, also called fitnesses, associated with each chromosome. This property of GA is called blindness. Then GA uses probabilistic transition rules, namely randomized operators, to guide its search. These four properties -use of parameter coding, search from a population, blindness to extra information rather than fitness function, and randomized operators- build together the mechanics of GA. Its operation simplicity makes GA much more powerful.

There are three randomized operators in the application of GA, which are, namely, reproduction, crossover and mutation. In reproduction process, individual chromosomes are copied according to their objective function values f, which means that chromosomes with a higher objective function value have higher probability of contributing more children in the next generation. The easiest algorithm to use in reproduction is the roulette-wheel parent selection technique, where each chromosome in the population has a roulette wheel slot proportional to its fitness. Roulette-wheel parent selection can be summarized by the following three-step algorithm:

a) Sum the fitnesses of all the chromosomes in the population.
b) Generate a random number between 0 and total fitness.
c) If a chromosome in the population satisfies the criteria that its fitness added to fitnesses of the preceding population members is greater than or equal to the number generated in (b), return that chromosome as a parent chromosome.

This algorithm is repeated until the number of reproductions is equal to the number of chromosomes in the population. With this algorithm, chromosomes with higher fitnesses have higher number of children in the next generation. The

chromosomes selected in reproduction are then put into a pool, called mating pool, in order to generate a new population.

In crossover process, the chromosomes in the mating pool are mated at random and then each chromosome pair is crossed, where the parent chromosomes exchange parts of their chromosomes. This way, genetic material of the two parent chromosomes is recombined. Simple crossover, also called one point crossover, selects a random point and swaps the parts of the two parent chromosomes after this random point, and creates two children, if the probability test is passed. In the probability test, a number between 0 and 1 is chosen as crossover probability. If number selected randomly from this range exceeds crossover probability, crossover is applied to that pair. Crossover can also be performed at multiple points.

The last operator is mutation that is applied to recover the loss of some genetic material that may be useful. Mutation simply means changing a 1 in a chromosome to 0, and a 0 to 1, if that particular chromosome passes the probability test. The probability test is similar to the one performed in crossover.

Since genetic algorithm deals with the chromosomes that have higher fitnesses, it finds the global maximum of an objective function f_{obj}. To be able to use GA, the values of the objective function should be positive. The global minimum of an objective function f_{obj} can be found using $f_{obj}' = n - f_{obj}$ as the objective function where n is a positive number used to make f_{obj}' values all positive. Hence, GA may be applied to virtually any problem.

6.2 Optimization Results

In this thesis, GA is used to find the appropriate locations and widths of the shorting strips in a microstrip patch antenna to match the input impedances to 50Ω at both low and high frequencies and to satisfy a desired frequency ratio f_h/f_l. The reason for using genetic algorithm was mainly the complexity of the objective function, which makes the calculation of derivative impossible, and the parallel searching property of GA, which guarantees the determination of global maximum.

In the optimization, the feed location, its width and orientation, the number of shorting strips, their orientations and the desired frequency are used as known parameters. The unknown parameters of the optimization program are the x coordinate, y coordinate and the width of each shorting strip, which satisfy the desired frequency ratio in the dual frequency operation and provide perfect match to 50Ω for both bands. The objective function used is:

$$f_{obj} = 100 - \sqrt{\left(f_{ratio} - \frac{f_h}{f_l}\right)^2 + \left(Z_l - 50\right)^2 + \left(Z_h - 50\right)^2} \qquad (6.1)$$

where $f_{ratio} = f_h/f_l$ is the desired frequency ratio, Z_l is the input impedance at f_l and Z_h is the input impedance at f_h. 100 is a number determined empirically to make f_{obj} positive.

The resonance frequencies and input impedances are calculated using multi-port analysis. Due to the very large computation time, the hybrid model is not used in determining the resonant frequencies and input impedances.

Two antennas are used in the dual frequency operation. The properties of the antennas are given in Table 6.1. The antennas are chosen to have the same properties as the ones used in the experiments. The lateral extension of the feed is in x-direction for both antennas.

antenna	a	b	h	ε_r	σ	δ	x_p	y_p	d
#1	8.0	10.0	0.6	1	10^5	10^{-5}	4.0	0.0	0.5
#2	5.0	6.0	0.6	1	10^5	10^{-5}	2.5	0.0	0.5

Table 6.1: Properties of the antennas used in the optimization. All dimensions are in cm, the unit of σ is mho/cm.

The GA has five internal properties: chromosome length, population size, generation number, crossover probability, and mutation probability. In this thesis, the chromosome length is chosen as 25 chromosomes per unknown parameter. This way, the total length of each chromosome for a patch with N shorting strips is $3Nx25$. The crossover probability and mutation probability used are 0.65 and 0.008, respectively. Two-point crossover is applied in each trial. The population size and generation number determine the speed and efficiency of the genetic algorithm. Table 6.2 gives optimization results for the first antenna for different population size and generation number with at most 2 shorting strips. The limits of x and y points are determined by the patch dimensions. The limits for the strip widths are chosen as 0.1 cm - 1.5 cm. Here (x_{s1}, y_{s1}) is the location of the first strip and (x_{s2}, y_{s2}) is the location of the second strip. d_{s1} and d_{s2} are widths of the strips. P is the population size, G is the generation number and f_{ratio} is the desired frequency ratio. In the first case, the shorting strip is x directed. In the second case, both of the strips are x directed. In the last case, the first strip is chosen x directed and the second strip y directed.

Case	P	G	f_{ratio}	strip #	x_{s1}	y_{s1}	d_{s1}	x_{s2}	y_{s2}	d_{s2}
1	200	200	2.24	1	3.73	4.99	1.43	-	-	-
2	150	150	2.24	2	4.35	5.15	0.36	3.01	2.13	1.24
3	10^3	100	2.24	2	3.76	5.05	1.25	3.65	4.94	1.13

Table 6.2: Optimization results for the first antenna. Dimensions are in cm.

The locations and widths obtained in the simulations are tested using both multi-port analysis and hybrid model, and the results are tabulated in Table 6.3.

Model	Case #	f_l(GHz)	$\|\Gamma in\|_l$	f_h(GHz)	$\|\Gamma in\|_h$	f_h/f_l
Multi-port	1	1.7	0.041	3.95	0.008	2.32
	2	1.74	0.032	4.05	0.017	2.33
	3	1.74	0.041	4.11	0.002	2.36
Hybrid	1	1.69	0.163	4.0	0.073	2.37
	2	1.73	0.077	4.06	0.044	2.35
	3	1.74	0.179	4.15	0.006	2.38

Table 6.3: Resonant frequency results for the first antenna.

The optimization results corresponding to the second antenna are given in Table 6.4. The limits for the strip widths are chosen as 0.1 cm - 1 cm. The resonant frequencies found by the hybrid model and multi-port analysis using optimization results are tabulated in Table 6.5. The orientations of the strips are the same as the orientations of the first antenna.

Case	P	G	f_{ratio}	strip #	x_{s1}	y_{s1}	d_{s1}	x_{s2}	y_{s2}	d_{s2}
1	200	200	2.3	1	1.79	2.34	0.99	-	-	-
2	10^3	200	2.3	2	2.33	3.21	0.99	1.11	2.31	0.96
3	10^3	100	2.3	2	2.15	2.93	0.95	2.08	2.79	0.93

Table 6.4: Optimization results for the second antenna. Dimensions are in cm.

Model	Case #	f_l(GHz)	$\|\Gamma in\|_l$	f_h(GHz)	$\|\Gamma in\|_h$	f_h/f_l
Multi-port	1	2.53	0.093	6.13	0.200	2.42
	2	2.63	0.092	6.15	0.199	2.34
	3	2.61	0.039	6.11	0.178	2.34
Hybrid	1	2.53	0.141	6.16	0.164	2.43
	2	2.62	0.146	6.17	0.113	2.35
	3	2.64	0.071	6.11	0.210	2.31

Table 6.5: Resonant frequency results for the second antenna.

In both of the antennas, it is observed that the strip locations generally converge to the nodal *E* field lines. The frequency ratios that are too close to the desired frequency ratios and the input reflection coefficients that are close to zero justify the success of the optimization with genetic algorithm. The algorithm has been run for several initial populations, population size and generation number. The results tabulated in Table 6.2 and Table 6.4 are the ones that give the best match to the desired frequency ratio and to *50Ω*. In the optimizations, it is observed that the main disadvantage of genetic algorithm is its long computation time. Besides the choice of population size and generation number affect the success and efficiency of the algorithm. Low numbers of population size cause convergence to local optima and high generation numbers speed down the algorithm.

Chapter 7

Conclusion

In this thesis, a hybrid model that is developed for the analysis of vertical conductors in probe-fed rectangular microstrip antennas is presented. This model analyzes the effect of conductor structure of the feed and determines the field distribution under the microstrip patches with shorting strips. It considers the shorting strips as current sources with unknown current densities. The current densities are calculated using point matching application and the resulting field distribution is determined using cavity model.

The conventional method in evaluating the effect of shorting pins on the resonant frequencies was multi-port analysis that gives no information on the field distribution under the patch. The results of multi-port analysis and hybrid model are compared with the experimental results for both antennas with wide vertical feeds and antennas with shorting strips.

The resonant frequencies determined with the new model corresponding to both low band and high band operations are in good agreement with both the multi-port analysis and experiment results. The maximum error obtained is 0.93% for antennas without shorting strips and 3.65% for antennas with shorting strips. The input impedance patterns obtained by the hybrid model are in good agreement with the measured input impedance patterns. In addition, the field distribution found by the new model satisfies the zero tangential electric field condition on the shorting strips successfully. This model also decreases magnitude of the tangential electric field on the feed conductor.

Next, the locations and widths of the shorting strips are optimized using genetic algorithm to achieve desired frequency ratio and perfect match to 50Ω at both bands of operation for fixed feed location and feed width. Then these strip locations and widths are tested in both hybrid model and multi-port analysis. The frequency ratios and input reflection coefficients obtained were very close to the desired ones.

The only disadvantage of the hybrid model is its long computation time. Since it calculates the double summations in the field formulas at each frequency, calculations take long time. As a future work, hybrid model can be speeded up by the reduction of the double summations into single summations.

REFERENCES

[1] G. A. Deschamps, "Microstrip microwave antennas," presented at the 3rd USAF Symp. on Antennas, 1953.

[2] E. V. Byron, "A new flush-mounted antenna element for phased array application," in Proc. Phased-Array Antenna Symp., pp. 187-192, 1970.

[3] R. E. Munson, "Single slot cavity antennas assembly," U. S. Patent No. 3714162, Jan. 23, 1973.

[4] J. Q. Howell, "Microstrip antennas," in Dig. Int. Symp. Antennas Propagat. Soc., Williamburg, VA, pp. 177-180, Dec. 1972.

[5] R. E. Munson, "Conformal microstrip antennas and microstrip phased arrays," *IEEE Trans. Antennas and Propagation*, Vol. AP-22, no. 1, pp. 74-78, Jan. 1974.

[6] A. G. Derneryd, "Linear microstrip array antennas," Chalmer Univ. Technol., Goteborge, Sweden, Tech. Rep. TR 7505, Oct. 1975.

[7] Y. T. Lo, D. D. Harrison, D. Solomon, G. A. Deschamps, and F. R. Ore, "Study of microstrip antennas, microstrip phased arrays, and microstrip feed

networks," Rome Air Development Center, Tech. Rep. TR-77-406, Oct. 21, 1977.

[8] A. G. Derneryd, "A technical investigation of the rectangular microstrip antenna element," Rome Air Development Center, Tech. Rep. TR-77-206, June 1977.

[9] L. C. Shen, and S. A. Long, "Low Profile printed circuit antennas, " Dept. Elec. Eng., Univ. Houston, Houston, TX, Contract DAAG-29-75-0187, Final Rep. ,Oct. 1977.

[10] K. R. Carver, and E. L. Coffey, "Theoretical Investigation of the microstrip antenna, " Physic. and Sci. Lab., New Mexico State Univ., Las Cruces, Tech. Rep. PT-00929, Jan. 23, 1979.

[11] I. J. Bahl, and P. Bhartia, *Microstrip Antennas*, Artech House, Dedham, MA, 1980.

[12] K. R. Carver, and J. W: Mink, "Microstrip antenna technology," *IEEE Trans. Antennas and Propagation*, Vol. AP-29, pp. 2-24, 1981.

[13] K. Chang, *Handbook of Microwave and Optical Components*, Vol. 1, John Wiley & Sons, Inc., 1989.

[14] J. Huang, "Microstrip antennas for commercial applications," Jet Propulsion Lab., California Inst. of Tech., Pasadena.

[15] P. S. Hall, C. Wood, and C. Garrett, "Wide bandwidth microstrip antennas for circuit integration," *Electron. Letters*, Vol. 15, pp. 458-460, 1979.

[16] C. Wood, "Improved bandwidth of microstrip antennas using parasitic elements," *Proc. IEEE*, Vol. 127, Pt. H. pp. 231-234, 1980.

[17] H. F. Pues, and A. R. Van de Capelle, "Wideband impedance-matched microstrip resonator antennas," IEEE Second Inter. Conf. on Ant. and Propagation, Pt. 1, pp. 402-405, 1981.

[18] G. G. Sanford, and R. E. Munson, "Conformal VHF antenna for Apollo-Soyuz test project," IEEE AP-S Int. Symp. Digest, pp. 113-116, Oct. 1976.

[19] A. G. Derneryd, "Microstrip disc antenna covers multiple frequencies," *Microwave J.*, pp. 77-79, May 1978.

[20] D. H. Shaubert, F. G. Garrar, A. Sindoris, and S.T. Hayes, "Microstrip antennas with frequency agility and polarization diversity," *IEEE Trans. Antennas and Propagation*, Vol. 29, pp. 118-123, Jan. 1981.

[21] Y. T. Lo, C. E. Skupien, and S. S. Zhong, "A study of microstrip antennas for multiple band operation," Rep. RADC-TR-82-236, Sept. 1982.

[22] Y. T. Lo, C. E. Skupien, S. S. Zhong, and W. F. Richards, "Dual frequency microstrip antennas," Nat. Radio Sci. Meeting Digest, URSI, Houston, TX, p. 98, 1983.

[23] S. C. Pan, and K. L. Wand, "Dual frequency triangular microstrip antenna with a shorting pin," *IEEE Trans. Antennas and Propagation*, Vol. 45, pp. 1889-1891, 1997.

[24] R. B. Waterhouse and N. V. Shuley, "Dual frequency microstrip rectangular patches," *Electron. Lett.*, Vol. 28, pp. 606-607, 26 March 1992.

[25] S. Maci, G. B. Gentili, and G. Avitabile, "Single layer dual frequency patch antenna," *Electron. Lett.*, Vol. 29, pp. 1441-1443, 5 Aug. 1993.

[26] Y. M. M. Antar, A. I. Ittipiboon, and A. K. Bhattacharyya, "A dual frequency antenna using a single patch and an inclined slot," *Microwave Opt. Technol. Lett.*, Vol. 8., pp. 309-311, 20 April 1995.

[27] H. D. Chen, "A dual frequency rectangular microstrip patch antenna with a circular slot," *Microwave Opt. Technol. Lett.*, Vol. 18, pp. 130-132, June 5 1998.

[28] K. L. Wong, and G. B. Hsieh, "Dual-frequency circular microstrip antenna with a pair of arc-shaped slots," *Microwave Opt. Technol. Lett.*, Vol. 19, pp. 410-412, 20 Dec. 1998.

[29] K. L. Wong, M. C. Pan, and W. H. Hsu, "Single-feed dual-frequency triangular microstrip antenna with a V-shaped slot," *Microwave Opt. Technol. Lett.*, Vol. 20, pp. 133-134, 20 Jan. 1999.

[30] J. H. Lu, "Novel dual-frequency design of single-feed equilateral-triangular microstrip antenna," *Microwave Opt. Technol. Lett.*, Vol. 22, pp. 133-136, 20 July 1999.

[31] J. Y. Jan, and K. L. Wong, "Single-feed dual-frequency circular microstrip antenna with an open-ring slot," *Microwave Opt. Technol. Lett.*, Vol. 22, pp. 157-160, 5 Aug. 1999.

[32] J. H. Lu, and K. L. Wong, "Compact dual-frequency circular microstrip antenna with an offset circular slot," *Microwave Opt. Technol. Lett.*, Vol. 22,

pp. 254256, 20 Aug. 1999.

[33] S. T. Fang, and K. L. Wong, "A dual-frequency equilateral-triangular microstrip antenna with a pair of narrow slots," *Microwave Opt. Technol. Lett.*, Vol. 23, pp. 82-84, 20 Oct. 1999.

[34] J. H. Lu, "Dual-frequency operation of a single-feed rectangular microstrip antenna with a pair of comb-shaped slots," *Microwave Opt. Technol. Lett.*, Vol. 23, pp. 183-186, 5 Nov. 1999.

[35] J. H. Lu, "Slot-loaded rectangular microstrip antenna for dual-frequency operation," *Microwave Opt. Technol. Lett.*, Vol. 24, pp. 234-237, 20 Feb. 2000.

[36] G. S. Binoy, C. K. Aanandan, P. Mohanan, K. Vasudevan, and K. G. Nair, "Single-feed dual-frequency dual-polarized slotted square microstrip antenna," *Microwave Opt. Technol. Lett.*, Vol. 25, pp. 395397, 20 June 2000.

[37] Y. X. Guo, K. M. Luk, and K. F. Lee, "A dual-band patch antenna with two U-shaped slots," *Microwave Opt. Technol. Lett.*, Vol. 26, pp. 73-75, 20 July 2000.

[38] K. L. Wong, and S. T. Fang, "Reduced-size circular microstrip antenna with dual-frequency operation," *Microwave Opt. Technol. Lett.*, Vol. 18, pp. 54-56, May 1998.

[39] K. L. Wong, S. T. Fang and J. H. Lu, "Dual frequency equilateral-triangular microstrip antenna with a slit," *Microwave Opt. Technol. Lett.*, Vol. 19, pp. 348-350, 5 Dec. 1998.

[40] J. F. Zürcher, A. Skrivervik, O. Staub, and S. Vaccaro, "A compact dual-port dual-frequency printed antenna with high decoupling," *Microwave Opt. Technol. Lett.*, Vol. 19, pp. 131-137, 5 Oct. 1998.

[41] J. F. Zürcher, Q. Xu, A. Skrivervik, and J. R. Mosig, "Dual-frequency, dual-polarization four port printed planar antenna," *Microwave Opt. Technol. Lett.*, Vol. 23, pp. 75-78, 20 Oct. 1999.

[42] M. Kijima, Y. Ebine, and Y. Yamada, "Development of a dual-frequency base station antenna for cellular mobile radios," *IEICE Trans. Commun.*, Vol. E82-B, pp. 636-643, 4 Apr. 1999.

[43] B. F. Wang, and Y. T. Lo, "Microstrip antennas for dual-frequency operation," *IEEE Trans. Antennas and Propagation*, Vol. AP-32, pp. 938-943, Sep. 1984.

[44] W. F. Richards, Y. T. Lo, and D. D. Harrison, "An improved theory for microstrip antennas and applications," *IEEE Trans. Antennas and Propagation*, Vol. AP-29, pp. 38-46, Jan. 1981.

[45] K. R. Carver, " A modal expansion theory of the microstrip antenna," IEEE AP-S Int. Symp. Digest, pp. 101-104, 1979.

[46] Y. T. Lo, D. Solomon, and W. F. Richards, "Theory and experiment on microstrip antennas," *IEEE Trans. Antennas and Propagation*, Vol. AP-27, pp. 137-145, March 1979.

[47] J. H. Newman, and P. Tulyathan, "Analysis of microstrip antennas using moment methods," *IEEE Trans. Antennas and Propagation*, Vol. AP-29, pp.

47-53, Jan. 1981.

[48] E. L. Coffey, and K R. Carver, "Towards the theory of microstrip antenna patterns," Proc. Ant. Appl. Symp., Univ. of Illinois, Urbana, IL, April 1977.

[49] K. R. Carver, and E. L. Coffey, "Technical Investigation of the microstrip antenna," Technical Report, PT-00929, Physical Science Laboratory, New Mexico State University, Las Cruces, NM, Jan. 1979.

[50] E. L. Coffey, "DFNA analysis of microstrip antenna," IEEE AP-S Int. Symp. Digest, pp. 613-616, 1980.

[51] P. K. Agrawal, and M. C. Bailey, "An analysis technique for microstrip antennas," *IEEE Trans. Antennas and Propagation*, Vol. AP-25, pp. 756-759, Nov. 1977.

[52] K. C. Gupta, and P. C. Sharma, "Segmentation and desegmentation techniques for an analysis of planar microstrip antennas," IEEE AP-S Int. Symp. Digest, pp. 19-22, 1981.

[53] T. Kashiwa, S. Koike, N. Yoshida, and I. Fukai, "Three-dimensional analysis of patch antenna by Bergeron's method," *Trans. IECE of Japan*, Vol. J71-B, pp. 576-584, April 1988.

[54] A. Reineix, and B. Jecko, "Analysis of microstrip patch antennas using finite difference time domain method," *IEEE Trans. Antennas and Propagation*, Vol. AP-37, pp. 1361-1369, Nov. 1989.

[55] D. R. Jackson, *Analysis and Design of Microstrip Antennas Short Course*, IEEE AP-S International Symp. and URSI National Radio Science Meeting,

1990.

[56] J. A. Kong, *Electromagnetic Wave Theory*, John Wiles & Sons, p. 393, 1986.

[57] D. K. Cheng, *Field and Wave Electromagnetics*, Ch. 10, Addison Wesley Publishing Company, 1989.

[58] M.Kara, "The resonant frequency of rectangular microstrip antenna elements with various substrate thicknesses," *Microwave Opt. Technol. Lett.*, Vol. 11, pp. 55-58, 5 Feb. 1996.

[59] W. F. Richards, and Y. T. Lo, "Theoretical and experimental investigation of a microstrip radiator with multiple lumped linear loads," *Electromagnetics*, Vol. 3, Nos. 3-4, pp. 371-385, July-Dec. 1983.

[60] D. Lee, and S. Lee, "Design of a coaxially fed circularly polarized rectangular microstrip antenna using a genetic algorithm," *Microwave Opt. Technol. Lett.*, Vol. 26, pp. 288-291, 18 Jul. 2000.

[61] T. Günel, "A fuzzy hybrid approach for the synthesis of rectangular microstrip antenna elements with thick substrates," *Microwave Opt. Technol. Lett.*, Vol. 26, pp. 351-355, 28 Jul. 2000.

[62] J. M. Johnson, and Y. Rahmat-Samii, "Genetic algorithms and method of moments (GA/MOM) for the design of integrated antennas," *IEEE Trans. Ant9ennas and Propagation*, Vol. 47, pp. 1606, Oct. 1999.

[63] F. J. Ares-Pena, J. A. Rodriguez-Gonzalez, E. Villaneuva-Lopez, and S. R. Rengarajan, "Genetic algorithms in the design and optimization of antenna

array patterns," *IEEE Trans. Antennas and Propagation*, Vol. 47, pp. 506, March 1999.

[64] Lale Alatan, M.I. Aksun, K. Leblebicioglu, and T. Birand, "Use of computationally efficient MoM in the optimization of printed structures," *IEEE Trans. Antennas and Propagation*, Vol. 47, pp. 725-732, April 1999.

[65] K. P. Ray, and G. Kumar, "Determination of the resonant frequency of microstrip antennas," *Microwave Opt. Technol. Lett.*, Vol. 23, pp. 114-117, 20 Oct. 1999.

APPENDIX A

Edge Extension Formulas for Rectangular Patch Antennas

For a microstrip patch antenna with the physical width W, physical length L, thickness h, dielectric constant ε_r, and strip conductor thickness t, the following frequency-dependent formulas are used for the calculation of edge extension Δl [65]. The effective dielectric constant $\varepsilon_{eff}(f)$ as a function of frequency is computed using the following expressions:

$$\varepsilon_{eff}(f) = \varepsilon_r - [(\varepsilon_r - \varepsilon_{eff}(0))/(1 + P)] \tag{A.1}$$

where $\varepsilon_{eff}(0)$ is the static effective dielectric constant, and is given by:

$$\varepsilon_{eff}(0) = \frac{1}{2[\varepsilon_r + 1 + (\varepsilon_r - 1)G]}$$

$$G = (1 + 10h/W)^{-AB} - \left[(\ln 4/\pi)\cdot\left(t\cdot(Wh)^{-1/2}\right)\right]$$

$$A = 1 + \frac{1}{49}\ln\left[\frac{(W/h)^4 + W^2/(52h)^2}{(W/h)^4 + 0.432}\right] + \frac{1}{18.7}\ln\left[1 + (W/18.1h)^3\right]$$

$$B = 0.564\exp[-0.2/(\varepsilon_r + 0.3)] \tag{A.2}$$

and

$$P = P_1 P_2 [(0.1844 + P_3 P_4) f_n]^{1.5763} \tag{A.3}$$

with

$$P_1 = 0.27488 + \{0.6315 + \{0.525/(1 + 0.0157 f_n)^{20}\}\}u - 0.065683\exp(-8.7513u)$$

$$P_2 = 0.33622[1 - \exp(-0.03442\varepsilon_r)]$$

$$P_3 = 0.0363\exp(-4.6u)\{1 - \exp[-(f_n/38.7)^{4.97}]\}$$

$$P_4 = 1 + 2.751\{1 - \exp[-(\varepsilon_r/15.916)^8]\}$$

$$f_n = 47.713kh, \qquad \text{where } k = 2\pi/\lambda_0$$

$$u = [W + (dW - W)/\varepsilon_r]/h$$

$$dW = W + \frac{t}{\pi}\left[1 + \ln\left\{\frac{4}{(t/h)^{1/2}} + \frac{(1/\pi)^2}{(W/t + 1.1)^2}\right\}\right].$$

The edge extension for the width W is computed using the following equation:

$$\Delta l = h\xi_1\xi_3\xi_5/\xi_4 \tag{A.4}$$

where

$$\xi_1 = 0.434907\frac{\varepsilon_{\text{eff}}(f)^{0.81} + 0.26}{\varepsilon_{\text{eff}}(f)^{0.81} - 0.189}\cdot\frac{(W/h)^{0.8544} + 0.236}{(W/h)^{0.8544} + 0.87}$$

$$\xi_2 = 1 + \frac{(W/h)^{0.371}}{2.358\varepsilon_r + 1}$$

$$\xi_3 = 1 + \frac{0.5274 \arctan\left[0.067(W/h)^{1.9413/\xi_2}\right]}{\varepsilon_{\text{eff}}(f)^{0.9236}}$$

$$\xi_4 = 1 + 0.0377 \arctan\left[0.067(W/h)^{1.456}\right] \times [6 - 5\exp\{0.036(1-\varepsilon_r)\}]$$

$$\xi_5 = 1 - 0.218\exp(-7.5W/h).$$

So, the effective width of the patch antenna is $W + 2\Delta l$. The effective length is obtained similarly by replacing W by L in all the above expressions.

APPENDIX B

Formulas for the Reduction of Double Infinite Summation into Single Infinite Summation

In the simulation of Cavity Model, double summation S, given in Eq. B.1 in the electric field expression is reduced into single summation form for speeding up the computations.

$$S = \sum_{m=0}^{\infty}\sum_{n=0}^{\infty} \frac{\psi_{mn}(x_1, y_1)\psi_{mn}(x_2, y_2)}{k^2 - k_{mn}^{\ 2}} \operatorname{sinc}\left(\frac{md}{2aN}\right) \tag{B.1}$$

Replacing

$$\psi_{mn}(x, y) = \left(\frac{\varepsilon_{om}\varepsilon_{on}}{ab}\right)^{1/2} \cos\left(\frac{m\pi x}{a}\right)\cos\left(\frac{n\pi y}{b}\right) \tag{B.2}$$

and reorganizing the resulting terms in the expression of S gives:

$$S = \sum_{m=0}^{\infty} \frac{\varepsilon_{om}}{ab} \cos\left(\frac{m\pi x_1}{a}\right) \cos\left(\frac{m\pi x_2}{a}\right) \operatorname{sinc}\left(\frac{md}{2aN}\right) sum(n) \tag{B.3}$$

where

$$sum(n) = \sum_{n=0}^{\infty} \frac{\varepsilon_{on} \cos\left(\frac{n\pi y_1}{b}\right) \cos\left(\frac{n\pi y_2}{b}\right)}{k_y^2 - \left(\frac{n\pi}{b}\right)^2} \tag{B.4}$$

and

$$k_y{}^2 = k^2 - \left(\frac{m\pi}{a}\right)^2 \tag{B.5}$$

ε_{on} is given by

$$\varepsilon_{on} = \begin{cases} 1 & if \quad n = 0 \\ 2 & if \quad n \neq 0 \end{cases} \tag{B.6}$$

Using the expression for ε_{on} and the trigonometric identity

$$\cos a \cos b = \frac{1}{2}\left(\cos(a-b) + \cos(a+b)\right) \tag{B.7}$$

sum(n) turns into the following form:

$$sum(n) = \frac{1}{k_y^2} - \frac{b^2}{\pi^2}\left(\sum_{n=1}^{\infty} \frac{\cos\left(\frac{n\pi}{b}(y_1 + y_2)\right)}{n^2 - \left(\frac{k_y b}{\pi}\right)^2} + \sum_{n=1}^{\infty} \frac{\cos\left(\frac{n\pi}{b}|y_1 - y_2|\right)}{n^2 - \left(\frac{k_y b}{\pi}\right)^2} \right) \tag{B.8}$$

The following summation formula that is obtained by contour integration is applicable in *sum(n)* expression:

$$\sum_{n=1}^{\infty} \frac{\cos(nx)}{n^2 - w^2} = \frac{1}{2w^2} - \frac{\pi \cos((x-\pi)w)}{2w\sin(\pi w)} \qquad \text{for } 0 \le x \le 2\pi \tag{B.9}$$

Applying Eq. B.9 to *sum(n)* and placing this equation into Eq. B.3, the final single summation form is obtained for *S*:

$$S = \sum_{m=0}^{\infty} \frac{\varepsilon_{om} \cos\left(\frac{m\pi x_1}{a}\right)\cos\left(\frac{m\pi x_2}{a}\right)\text{sinc}\left(\frac{md}{2aN}\right)}{2ak_y \sin(k_y b)} C \tag{B.10}$$

with

$$C = \left(\cos(k_y(y_1 + y_2) - k_y b) + \cos(k_y|y_1 - y_2| - k_y b)\right) \tag{B.11}$$

There are two other summation formulas that are used in the reduction of double summations of far-zone field expressions in the Cavity Model and input impedance expressions in both the Cavity Model and multi-port analysis into single summations. These are:

$$\sum_{n=1,3,\ldots}^{\infty} \frac{\cos(nx)}{n^2 - w^2} = \frac{\pi \sin\left(\left(\frac{\pi}{2} - x\right)w\right)}{4w\cos\left(\frac{\pi a}{2}\right)} \qquad \text{for } 0 \le x \le \pi \tag{B.12}$$

$$\sum_{n=1}^{\infty} \frac{\cos(nx)}{(n^2 - w^2)(n^2 - s^2)} = -\frac{1}{2w^2 s^2} - \frac{\pi}{2}\left[\frac{\cos((\pi - x)w)}{w(w^2 - s^2)\sin(\pi w)} + \frac{\cos((\pi - x)s)}{s(s^2 - w^2)\sin(\pi s)}\right]$$

$$\text{for } 0 \le x \le 2\pi \tag{B.13}$$